*Institute of Space and Aeronautical Science, University of Tokyo*
*Report No. 488, December 1972*

# Roll Coupling Moment of Deflected Wing-Body Combination

*By*

Shigeki TSUKAMOTO

*Summary*: A method of analysis based on the slender-body theory has been developed to investigate the characteristics of the roll coupling moment due to the flow induced by deflected wings and cross flow. The method makes use of conformal mapping of the well-known hydrodynamics and numerical integration. Flow patterns on the wing have been obtained in the form of elliptic integrals and are shown for various values of span to body radius ratio $\lambda$. Calculatios have been performed for uniformly canted and elastically deflected wings in planar and cruciform wing-body combinations. It is shown that there exists a considerably wide region (from the root to 50~57 percent of the wing span) where induced velocity has negative sign for the elastcially deffected wings. Roll coupling moment coefficients are also presented for wing-body combinations of various values of $\lambda$.

## CONTENTS



## SYMBOLS

$a$ radious of circular body
$c$ wing chord
$Cl$ rolling moment coefficient

$e$ nondimensional distance between elastic axis and center of pressure of wing

$E(\phi, k)$ incomplete elliptic integral of second kind of amplitude $\phi$ and modulus $k$

$E(k)$ complete elliptic integral of second kind

$F(\phi, k)$ incomplete elliptic integral of first kind of amplitude $\phi$ and modulus $k$

$K(k)$ complete elliptic integral of first kind

$GJ$ torsional rigidity of wing panel

$M_0$ free-stream Mach number

$p$ local static pressure

$p_0$ free-stream static pressure

$\Delta p$ $p-p_0$

$P$ pressure coefficient

$\Delta P$ difference in pressure coefficients

$q_0$ free-stream dynamic pressure

$s$ semispan of wing

$u, v, w$ perturbation velocity components along $x, y$ and $z$ axes

$V_0$ free-stream velocity

$W$ complex potential in $\mathscr{Z}$ plane

$\xi, \eta, \zeta$ coordinate axes fixed in the fluid

$x, y, z$ principal axes of symmetry of missile

$x', y', z'$ coordinate axes, in which $z'$-axis is in the direction of incident flow

$\mathscr{Z}$ $y+iz$

$\alpha$ angle of attack

$\alpha_c$ included angle between $V_0$ and missile longitudinal axis

$\beta$ angle of sideslip

$\gamma$ ratio of specific heats

$\delta$ local wing deflection

$\delta_1, \delta_2, \delta_3, \delta_4,$ deflections of horizontal and vertical wings

$\delta_a$ $(\delta_1-\delta_2)/2$

$\Lambda^2$ $q_0 c^2 e C_{L\alpha}/GJ$

$\lambda$ $s/a$

$\mu$ polar coordinate angle of the point in the $\sigma$ plane corresponding to the wing and body junction in the $\mathscr{Z}$ plane

$\sigma$ plane in which wing-body cross section transforms into unit circle

$\varphi$ velocity potential in $\xi, \eta, \zeta$ system

$\Phi$ velocity potential

$\varphi_\alpha, \varphi_\beta, \varphi_{\delta_e},$ velocity potentials associated with $\alpha, \beta, \delta_e, \delta_a, a,$

$\varphi_{\delta_a}, \varphi_a$ respectively

$\psi$ stream function

## 1. INTRODUCTION

The present paper deals with some kinds of the roll coupling moment in the wing-body combination, in which the wings are uniformly canted to the body longitudinal axis and/or deflected elastically by aerodynamic load. The problem will be approached on the basis of the slender body theory. An analysis of slender, lifting, planar wing-body and cruciform wing-body combinations was presented by Spreiter in Ref. 9. Theoretical investigation of roll characteristics of slender cruciform wings was also reported in Ref. 2. Several other analyses of rolling-moment characteristics of cruciform wing and wing-body combinations were made in the decade of 1950. Rebner treated the rolling cruciform wing with subsonic leading edges; Bleviss made an analysis for the case of the cruciform wing having supersonic leading edge; Graham [7] evaluated the rolling moment for the case of the cruciform wing-body combinations in the limiting case of an infinite number of fins; Tucker and Piland [8] developed a method of obtaining approximate linearized solutions for the damping in roll and calculated the approximate coefficient of damping in roll for configurations having rectangular and triangular wings.

Graymor and Dugan [5] have calculated the damping coefficient due to differential wing incidence for slender wings and wing-body combinations.

Qualitative explanations for the second order pitching (yawing) and rolling moment of various kinds can be found in Ref. 1.

The problem of the dynamic coupling in pitch and roll is important in the design of the spin-stabilized rocket, in which the spin is imparted to the vehicle by canting the tail fins. An example of this type of coupling is found in Ref. 4, which describes the flight behavior of a certain type of Aerobee sounding rocket. Spin rate increases with time in the powered flight while the frequency of pitch (precession) decreases and when the frequency of rolling motion coincides with the pitching motion, the spin ceases to increase, and even decreases, causing an abrupt change of flight direction with almost zero spin. This phenomenon is important from the view point of flight safety, but it has not been sufficiently understood yet. It is suggested in Ref. 4 that separation at wings, elastic deformation of wing and/or body, malalignment in wing attachment and/or thrust are mentioned as conceivable reasons for this dynamic coupling.

We assume a steady flight condition with a constant crossflow which is constant in magnitude and direction. The first order rolling moment produced by canted wings is considered to be in equilibrium while the second order rolling moment may play an important rôle when the precession rate and spinning rate coincide.

The present analysis considers the second order coefficient of rolling moment due to cross flow for wing incidence which is constant (case 1) or increasing (case 2) in span-wise direction. For cruciform wing-body combination, cross flow is different from that of planar wing-body combination, because of the panel interference, and these two cases are treated and compared in the present report.

The application of the slender body theory reduces the problem to that of finding the velocity potential of two dimensional flow of an incompressible fluid

about a cylinder with fins. The fins is replaced by uniform source and sink distribution in case-1, and by a distribution in which the strength of source and sink is increasing in span-wise direction in case-2. It is convenient to determine the potential by means of a source and sink distribution on a circle in the transformed plane.

## 2. Theoretical Formulation

### 2.1 *Basic equations*

Let the cartesian axes $\xi$, $\eta$, $\zeta$ be a set of axes fixed in the fluid. The pressure and density for the fluid are related through the isentropic law

$$\frac{p}{\rho^{\gamma}}=\text{const.} \tag{2-1}$$

$\gamma$ being the ratio of the specific heats.

Let $\varphi$ be the velocity potential function. The complete nonlinear equation for $\varphi$ is

$$\begin{aligned}\left[C_{\infty}^2-(\gamma-1)\left((\varphi_{\tau}^2+\frac{\varphi_{\xi}^2+\varphi_{\eta}^2+\varphi_{\zeta}^2}{2}\right)\right](\varphi_{\xi\xi}+\varphi_{\eta\eta}+\varphi_{\zeta\zeta})\\ =\varphi_{\tau\tau}+(\varphi_{\xi}^2\varphi_{\xi\xi}+\varphi_{\eta}^2\varphi_{\eta\eta}+\varphi_{\zeta}^2\varphi_{\zeta\zeta})\\ +2(\varphi_{\xi}\varphi_{\eta}\varphi_{\xi\eta}+\varphi_{\eta}\varphi_{\zeta}\varphi_{\eta\zeta}+\varphi_{\zeta}\varphi_{\xi}\varphi_{\zeta\xi})\\ +2(\varphi_{\xi}\varphi_{\xi\tau}+\varphi_{\eta}\varphi_{\eta\tau}+\varphi_{\zeta}\varphi_{\zeta\tau})\end{aligned} \tag{2-2}$$

The symbol $\tau$ represents time and $C_{\infty}$ is the speed of sound in the air at infinity.

With reference to Fig. 1–1, let $\bar{x}, \bar{y}, \bar{z}$, be axes fixed to the body at time $t$ and $\bar{x}$ be parallel to the uniform velocity $V_0$ of the fluid at infinity as seen from the body.

To obtain the potential equation in the $\xi, \eta, \zeta$ system to the $\bar{x}, \bar{y}, \bar{z}, t$ system, we transform the coordinates by following formula:

$$\begin{aligned}\bar{x}&=\xi+V_0\tau\\ \bar{y}&=\eta\\ \bar{z}&=\zeta\\ t&=\tau\end{aligned} \tag{2-3}$$

From the equation of $\varphi$ with respect to $\xi, \eta, \zeta, \tau$ we obtain a new equation for $\Phi$ which is related to $\varphi$ as

$$\Phi=V_0\bar{x}+\varphi \tag{2-4}$$

The new potential equation is;

$$\left[C_s^2-(\gamma-1)\left(\Phi_t+\frac{\Phi_x^2+\Phi_y^2+\Phi_z^2}{2}\right)\right](\Phi_{xx}+\Phi_{yy}+\Phi_{zz})$$
$$=\Phi_{tt}+(\Phi_x^2\Phi_{xx}+\Phi_y^2\Phi_{yy}+\Phi_z^2\Phi_{zz}) \qquad (2\text{–}5)$$
$$+2(\Phi_x\Phi_y\Phi_{xy}+\Phi_y\Phi_z\Phi_{yz}+\Phi_z\Phi_x\Phi_{zx})$$
$$+2(\Phi_x\Phi_{xt}+\Phi_y\Phi_{yt}+\Phi_z\Phi_{zt})$$

where

$$C_s^2=C_\infty^2+\frac{\gamma-1}{2}U_0^2$$

The sound velocity $C_s$ corresponds to stagnation condition. The velocity components are

$$\Phi_x=V_0+\bar{u}, \quad \Phi_y=\bar{v}, \quad \Phi_z=\bar{w} \qquad (2\text{–}6)$$

where $\bar{u}$, $\bar{v}$ and $\bar{w}$ are perturbation velocities. If we assume that the perturbation velocities are small compared to $V_0$ and neglect all the terms higher than the first order, then we can derive from Eq. (2–5) the linearized potential equation;

$$\Phi_{xx}(1-M_0^2)+\Phi_{yy}+\Phi_{zz}=\frac{1}{c^2}\Phi_{tt}+\frac{2M_0}{c}\Phi_{xt} \qquad (2\text{–}7)$$

where $M_0$ is free-stream Mach number.

Bernoulli's equation for the compressible potential flow in the $\xi, \eta, \zeta, \tau$ sytem can be expressed as:

$$\int\frac{dp}{\rho}+\varphi_\tau+\frac{q^2}{2}=C(\tau) \qquad (2\text{–}8)$$

where

$$q^2=\varphi_\xi^2+\varphi_\eta^2+\varphi_\zeta^2$$

For a steady flow with the pressure and density related by Eq. (2–1), Bernoulli's equation becomes

$$\frac{\gamma}{\gamma-1}\frac{p}{\rho}+\frac{q^2}{2}=\frac{\gamma}{\gamma-1}\frac{p_R}{\rho_R}+\frac{q_R^2}{2} \qquad (2\text{–}9)$$

We define the pressure coefficient $P$ as

$$P=\frac{p-p_0}{1/2\rho_0V_0^2} \qquad (2\text{–}10)$$

From Eqs. (2–9) and (2–10) we obtain

$$P\frac{\gamma M_\infty^2}{2}=\left[1-\frac{\gamma-1}{C_\infty^2}\left(\frac{q^2}{2}+\varphi_\tau\right)\right]^{\gamma/(\gamma-1)}-1 \qquad (2\text{–}11)$$

Expansion of Eq. (2–11) yields the power series:

$$P=-2\frac{q^2/2+\varphi_\tau}{U_0^2}+M_\infty^2\left(\frac{q^2/2+\varphi_\tau}{U_0^2}\right)^2+\cdots \tag{2–12}$$

This relation is expressed in terms of $\bar{u}$, $\bar{v}$ and $\bar{w}$ and the final result for steady flow is

$$P=\frac{-2\bar{u}}{V_0}+\frac{\bar{u}^2(M_0^2-1)-\bar{v}^2-\bar{w}^2}{V_0}+O\left(\frac{\bar{u}}{V_0}\right)^3 \tag{2–13}$$

If we assume that the body is sufficiently slender or $M_0=1$ equations to be solved are simplified as:

$$\Phi_{yy}+\Phi_{zz}=0 \tag{2–14}$$

$$P=-\frac{2\bar{u}}{V_0}-\frac{\bar{v}^2+\bar{w}^2}{V_0} \tag{2–15}$$

Eq. (2–14) is the two dimensional Laplace's equation.

### 2.2 *Coupling effects*

The linearized basic equations have been derived in the preceeding section.

The quadratic terms of the Bernoulli's equation are essential in calculating the coupling effect. An example of a coupling effect is the rolling moment originated by planar wings due to sideslip of body at a fixed angle of attack. Such a rolling moment is produced by interference between angle of attack $\alpha$ and sideslip $\beta$ and is proportional to $\alpha\beta$.

There are many kinds of coupling effects and some of them have been analyzed in Ref. 1. Here we will consider some types of coupling that occur between the effect of body thickness, angle of attack, angle of sideslip, symmetrical deflection of wing panels. We difine $\delta_e$ and $\delta_a$ as follows.

$$\begin{aligned}\delta_e&=\frac{\delta_1+\delta_3}{2}, & \delta_e'&=\frac{\delta_2+\delta_4}{2}\\ \delta_a&=\frac{\delta_1-\delta_3}{2}, & \delta_a'&=\frac{\delta_2-\delta_4}{2}\end{aligned} \tag{2–16}$$

where $\delta_1$, $\delta_2$, $\delta_3$ and $\delta_4$ are deflection angle of wings shown in Fig. (1–4). These may be function of $y$ or $z$. Trailing edge down is taken to be positive for $\delta_1$ and $\delta_3$. Positive values of $\delta_2$ and $\delta_4$ correspond to a movement of the trailing edges of the wings to the right.

As shown in Fig. (1–3), let us assume that the body longitudinal axis is inclined at angle $\alpha_c$ with freestream. Let the component of freestream velocity $V_0$ to the body longitudinal axis produce a perturbation potential $\varphi_a$. Let the velocity of crossflow $V_0\alpha_c$ be resolved into components $V_0\alpha$ and $V_0\beta$ as shown in Fig. (1–3), and $\varphi_\alpha$, $\varphi_\beta$ the perturbation potentials for unit velocity in $z$, $y$ directions, and $\varphi_{\delta_e}$,

$\varphi_{\delta_a}$ be the potentials for unit symmetrical and unit asymmetrical deflections of the horizontal wing.

The total perturbation potential can be written as a summation of each potential

$$\varphi=\varphi_a+\alpha\varphi_\alpha+\beta\varphi_\beta+\delta_e\varphi_{\delta_e}+\delta_a\varphi_{\delta_a} \tag{2-17}$$

The pressure coefficient $P$ can be given by Eq. (2-15)

$$\begin{aligned} P&=\frac{p+p_0}{(1/2)\rho_0 V_0^2}\\ &=-2\left(\frac{\partial\varphi}{\partial x}+\alpha\cos\varphi\frac{\partial\varphi}{\partial z}-\alpha\sin\varphi\frac{\partial\varphi}{\partial y}\right)-\left[\left(\frac{\partial\varphi}{\partial y}\right)^2+\left(\frac{\partial\varphi}{\partial z}\right)^2\right] \end{aligned} \tag{2-18}$$

We will calculate the coupling effects on the basis of this equation. The local pressure difference across the horizontal and vertical wings are given by $[P]$, which denotes the difference of $P$ on the lower and upper sides of wing. The symmetry properties of the velocity components and body-wing boundary conditions considerably simplify the results. To distinguish two sides of the wing panel, we put superscript + to the velocity components and pressure on the lower side of horizontal panel and superscript − to the same quantities on the upper side. In considering body-wing boundary conditions and the symmetry properties of velocity components, the relation between the perturbation velocities on the upper and lower sides can be expressed as follows:

$$\begin{array}{lllll} u_a^+=u_a^- & u_\alpha^+=-u_\alpha^- & u_\beta^+=u_\beta^- & u_{\delta_e}^+=-u_{\delta_a}^- & u_{\delta_a}^+=-u_{\delta_a}^-\\ v_a^+=v_a^- & v_\alpha^+=-v_\alpha^- & v_\beta^+=v_\beta^- & v_{\delta_e}^-=-v_{\delta_e}^- & v_{\delta_a}^+=-v_{\delta_a}^-\\ w_a^+=-w_a^- & w_\alpha^+=w_\alpha^- & w_\beta^+=w_\beta^- & w_{\delta_a}^+=w_{\delta_e}^- & w_{\delta_a}^+=w_{\delta\bar{x}}^-\\ =\left(\dfrac{dz}{dx}\right)^+ & =1 & =0 & =-1 & =\pm 1 \end{array} \tag{2-19}$$

Here complex sign $\pm$ in $\delta_a$ expression means that − sign refers to the right panel and + sign refers to the left panel. For the lower surfaces of the horizontal panels, the velocity components are

$$\begin{aligned} u^+&=u_a^+ +\alpha u_\alpha^+ +\beta u_\beta^+ +\delta_e u_{\delta_e}^+ +\delta_a u_{\delta_a}^+\\ v^+&=v_a^+ +\alpha v_\alpha^+ +\beta v_\beta^+ +\delta_e v_{\delta_e}^+ +\delta_a v_{\delta_a}^+\\ w^+&=\left(\frac{dz}{dx}\right)^+ -\alpha-\delta_e\mp\delta_a \end{aligned} \tag{2-20}$$

and for the upper surfaces of the horizontal panels, the velocity components are

$$\begin{aligned} u^-&=u_a^+ -\alpha u_\alpha^+ +\beta u_\beta^+ -\delta_e u_{\delta_e}^+ -\delta_a u_{\delta_a}^+\\ v^-&=v_a^+ -\alpha v_\beta^+ +\beta v_\beta^+ -\delta_e v_{\delta_e}^+ -\delta_a v_{\delta_a}^+\\ w^-&=-\left(\frac{dz}{dx}\right)^+ -\alpha-\delta_e\mp\delta_a \end{aligned} \tag{2-21}$$

The pressure coefficients for the lower and upper surfaces are

$$\begin{aligned} P^+ &= -2(u^+\alpha_e w^+ \cos\varphi - \alpha_e v^+ \sin\varphi) - (v^{+2}+w^{+2}) \\ P^- &= -2(u^- + \alpha_e w^- \cos\varphi - \alpha_e v^- \sin\varphi) - (v^{-2}+w^{-2}) \end{aligned} \tag{2-22}$$

The pressure difference on the horizontal panel is given by

$$\begin{aligned} [P] &= P^+ - P^- \\ &= -4\alpha u_\alpha^+ - 4\delta_e u_{\delta_a}^+ - 4\delta_a u_{\delta_a}^+ - 4\alpha v_\alpha^+ v_\alpha^+ + 4\beta(1-v_\beta^+)\alpha v_\alpha^+ \\ &\quad + 4\beta\delta_e(1-v_\beta^+)v_{\delta_e}^+ + 4\alpha\beta(1-v_\beta)v_\alpha^+ \\ &\quad + 4\delta_e\left[\left(\frac{dz}{dx}\right)^+ - v_{\delta_e}^+ v_\alpha^+\right] + 4\delta_a\left[\pm\left(\frac{dz}{dx}\right)^+ - v_{\delta_a}v_\alpha^+\right] \end{aligned} \tag{2-23}$$

The first three terms are linear, representing the effects of angle of attack, pitching and rolling. The others are the coupling terms. A similar expression is obtained for the vertical wings.

$$\begin{array}{lllll} u_\alpha^+ = u_\alpha^- & u_\alpha^+ = u_\alpha^- & u_\beta^+ = -u_\beta^- & u_{\delta_e}^+ = -u_{\delta_e}^- & u_{\delta_a}^+ = -u_{\delta_a}^- \\ v_\alpha^+ = -v_\alpha^- & v_\alpha^+ = v_\alpha^- & v_\beta^+ = -v_\beta^- & v_{\delta_e}^+ = v_{\delta_e}^- & v_{\delta_a}^+ = v_{\delta_a}^- \\ = \left(\dfrac{dy}{dx}\right)^+ & = 0 & = 1 & = 0 & = 0 \\ w_\alpha^+ = w_\alpha^- & w_\alpha^+ = w_\alpha^- & w_\beta^+ = -w_\beta^- & w_{\delta_e}^+ = w_{\delta_e}^- & w_{\delta_a}^+ = -w_{\delta_a}^- \end{array} \tag{2-24}$$

and the pressure difference for the vertical wings is also given by:

$$\begin{aligned} [P] = &-4\beta u_\beta^+ - 4\delta_a u_{\delta_a}^+ - 4\beta w_\beta^+ w_\alpha^+ \\ &- 4\delta_a w_{\delta_a}^+ w_\alpha^+ - 4\delta_e \beta w_{\delta_e}^+ w_\beta^+ \\ &- 4\alpha\beta w_\beta^+(1+w_\alpha^+) - 4\alpha\delta_a w_{\delta a}(1+w_\alpha^+) \\ &- 4\delta_e\delta_a w_{\delta_a}^+ w_{\delta_e}^+ \end{aligned} \tag{2-25}$$

For the cruciform wings, the same argument can be developed and the results are summarized in Table 1. There are three types of coupling moment in roll as shown in Table 1, *i.e.* $\alpha\beta$ coupling, $\beta\delta_e$ coupling and the coupling between angle of asymmetrical deflection and the effect of body thickness. In Ref. 1 $\alpha\beta$ coupling is analyzed in detail. The coupling between angle of asymmetrical deflection and the effect of body thickness is considered to be canceled by roll damping effect in equilibrium condition. We will focus the study on $\beta\delta_e$ coupling in the present paper.

## 3. Calculation of Potential for Cross Coupling

Let us calculate the perturbation potentials $\varphi_\beta$ and $\varphi_{\delta_e}$ to find the $\beta$-$\delta_e$ coupling term. Conformal mapping is useful for obtaining a potential about some cross section from the known flow about circular cross section. Here we transform a planar wing or a cruciform wing in physical plane of complex variable $\mathscr{Z}=y+iz$ to a circle in the

transformed plane of the complex variable $\sigma=\xi+i\eta$.

The transformation equation from planar mid-wing and body combination into a circle is written as;

$$\mathscr{Z}+\frac{a^2}{\mathscr{Z}}=\frac{1}{2}\left(s+\frac{a^2}{s}\right)\left(\frac{\sigma}{R}+\frac{R}{\sigma}\right),\qquad \frac{1}{2}\left(s+\frac{a^2}{s}\right)=R \tag{3-1}$$

where $s$ denotes semi-span length of a wing and $a$ denotes radius of body. Without loss of generality, we put $R=1$ for brevity. Then the right side of the first of the Eqs. (3–1) is reduced to $\sigma+R^2/\sigma$.

Two-dimensional incompressible flows are described by the two functions of a real variable, the potential function $\varphi$ and the stream function $\psi$ which can be described by the complex potential function $W(\mathscr{Z})$ defined by

$$W(\mathscr{Z})=\varphi=i\psi \tag{3-2}$$

If the velocity components parallel to the $y$ and $z$ axis are denoted by $v$ and $w$, these are related to the complex potential as follows:

$$\begin{aligned}&\frac{dW}{d\mathscr{Z}}=v+iw\\&\frac{\partial\varphi}{\partial y}=\frac{\partial\psi}{\partial z}=v\\&\frac{\partial\varphi}{\partial z}=-\frac{\partial\psi}{\partial y}=w\end{aligned} \tag{3-3}$$

The complex potential $W(\mathscr{Z})$ in the $\mathscr{Z}$ plane can be transformed to the complex potential $W_1(\sigma)$ in the $\sigma$ plane by employing the transformation relation. If the flow field at infinity is undistorted, the direct relation of velocity components in $\mathscr{Z}$ plane and $\sigma$ plane is

$$\begin{aligned}v_1-iw_1&=\frac{dW_1}{d\sigma}=\frac{dW}{d\mathscr{Z}}\frac{d\mathscr{Z}}{d\sigma}\\&=(v-iw)\left|\frac{d\mathscr{Z}}{d\sigma}\right|\exp\left(i\arg\frac{d\mathscr{Z}}{d\sigma}\right)\\&=v-iw\end{aligned} \tag{3-4}$$

This equation insures that the tangency condition at fixed boundaries is maintained during the transformation.

Now consider the planar wing-body combination at zero angle of bank. We assume that wings lie on $y$ axis. The uniform flow is assumed to be in the direction of z axis. The complex potential for circular cylinder in uniform flow in $\sigma$ plane is

$$W(\sigma)=-iV_0\left(\sigma-\frac{1}{\sigma}\right) \tag{3-5}$$

The complex perturbation potential due to angle of attack is given by Eqs. (3–1), (3–5) and

$$W_\alpha(\mathscr{Z}) = -iV_0\left\{\left[\left(\mathscr{Z}+\frac{1}{\mathscr{Z}}\right)^2-\left(s+\frac{a^2}{s}\right)^2\right]^{1/2}-\mathscr{Z}\right\} \tag{3–6}$$

Velocity component on $z$ axis for unit cross flow is given by performing differentiation on $W_\alpha$ by $\mathscr{Z}$ and set $\mathscr{Z}$ equal to $z$.

$$\begin{aligned} w_\alpha &= \mathrm{Re}\left\{\left(\frac{dW}{d\mathscr{Z}}\right)_{\mathscr{Z}=z}\right\} \\ &= 1-\frac{z\left(1-\dfrac{a^4}{z^4}\right)}{\left[\left(s+\dfrac{a^2}{s}\right)^2+\left(z-\dfrac{a^2}{z}\right)^2\right]^{1/2}} \end{aligned} \tag{3–7}$$

When the uniform flow is assumed to be in the direction of $y$ axis, we can obtain $v_\beta$ in the same way as:

$$v_\beta = \frac{a^2}{y^2} \tag{3–7}$$

These perturbation velocities will be used for determining the pressure difference on cruciform and planar wing.

In the previous section the expressions are presented for the perturbation potentials $\varphi$ induced by the deflection of wings. Here we apply again the method of conformal mapping to obtain the concrete formula of the perturbation potentials $\varphi_{\delta_e}$. The author has considered two cases of $\varphi_{\delta_e}$. One is that the deflection angle is constant along $y$ axis. (case-1) This case can be seen in the missile configuration, in which the attitude of the missile is controlled by varying the deflection angle of wings. The other is that the deflection angle is increasing along $y$ axis. (case-2). This case will be discussed later.

*Case-1* If a source and a sink of strength $m$ are located on the circumference of a circle shown in Fig. (1–6), then the circle is a stream-line of the resulting flow. The source and sink will be transformed into "doublet" located in line segment on $y$ axis, if the flow is transformed into $z$ plane by means of Eq. (3–1). The flow induced by the doublet at $y_0$ is normal to $y$ axis and at all other region on the line segment normal velocity is zero. This means that wing surfaces are stream-lines with the exception of the $y_0$ and the boundary conditions are satisfied. In the $\sigma$ plane the complex potential of the source and sink located at $\sigma=e^{i\theta_0}$ and $\sigma=e^{-i\theta_0}$ is

$$W = \frac{m}{2\pi}\log\frac{\sigma-e^{i\theta_0}}{\sigma-e^{-i\theta_0}} \tag{3–8}$$

At the corresponding point in $\mathscr{Z}$ plane $\mathscr{Z}=y_0$, there is outflow of $m/2$ above $y$ axis

and inflow of $m/2$ below $y$ axis. The flow across infinitesimal length $dy_0$ is $w(y_0)dy_0$, therefore, by continuity equation of flow

$$dm=2wdy_0 \tag{3-9}$$

From Eq. (3-3), we have

$$dm=2wdy_0=-2\frac{\partial\psi}{2\partial y_0}dy_0=-2d\psi \tag{3-10}$$

The potential for distributed doublet on circumference of the circle is given by integration from $\theta_0=0$ to $\theta_0=\mu$,

$$W(\sigma)=-\frac{1}{\pi}\int_{\theta_0=0}^{\theta_0=\mu}\log\frac{\sigma-e^{i\theta_0}}{\sigma-e^{-i\theta_0}}d\theta_0 \tag{3-11}$$

where $\mu$ denotes the polar angle of the point in the $\sigma$ plane corresponding to horizontal wing and body juncture. We substitute $\sigma=e^{i\theta}$ in Eq. (3-11). Integration is performed by part, and

$$W(\sigma)=-\frac{1}{\pi}\left[\psi(\mu)\log\frac{e^{i\theta}-e^{i\mu}}{e^{i\theta}-e^{-i\mu}}+\psi(\mu+\pi)\log\frac{e^{i\theta}-e^{i(\pi+\mu)}}{e^{i\theta}-e^{-i(\pi+\mu)}}\right.$$
$$\left.-\int_0^{\mu}\frac{\psi[\sin\theta+i(\cos\theta-\cos\theta_0)]}{\cos\theta-\cos\theta_0}d\theta_0-\int_{\pi}^{\pi+\mu}\frac{\psi[\sin\theta+i(\cos\theta-\cos\theta_0)]}{\cos\theta-\cos\theta_0}d\theta_0\right] \tag{3-12}$$

where imaginary constant has been omitted.
We denote the real part of the complex potential by $\varphi$, and in consideration of the reflective symmetry of doublet distribution.

$$\psi(\pi+\theta_0)=-\psi(\theta_0) \tag{3-13}$$

The velocity potential $\varphi(\theta)$ can be expressed as

$$\varphi(\theta)=-\frac{1}{\pi}\left[\psi(\mu)\log\frac{(e^{i\theta}-e^{i\mu})(e^{i\theta}+e^{-i\mu})}{(e^{i\theta}-e^{-i\mu})(e^{i\theta}+e^{i\mu})}\right]$$
$$-\frac{2\sin\theta}{\pi}\int_0^{\mu}\frac{\psi(\theta_0)\cos\theta_0}{\cos^2\theta-\cos^2\theta_0}d\theta_0 \tag{3-14}$$

for all value of $\theta$.

From the equation of transformation Eqs. (3-1) and (3-10), $\psi(\theta_0)$ can be expressed in term of $\theta_0$ as

$$\psi(\theta)=V\delta_e y_0=V\delta_e(\cos\theta_0+\sqrt{\cos^2\theta_0-\cos^2\mu})$$
$$\psi(\mu)=V\delta_e\cos\mu \tag{3-15}$$

Substituting Eq. (3-15) into Eq. (3-14) and after some calculation, the velocity potential $\varphi$ is expressed by

$$\varphi(\theta)=-\frac{V\delta_e}{\pi}\left[-2a\ \mathrm{arctanh}\left(\frac{\sin\theta}{\sin\mu}\right)\right.$$
$$\left.-2\sin\theta\left(\int_0^{\mu}\frac{\cos^2\theta_0 d\theta_0}{\cos^2\theta-\cos^2\theta_0}-\int_0^{\mu}\frac{\sqrt{\cos^2\theta_0-\cos^2\mu}}{\cos^2\theta-\cos^2\theta_0}d\theta_0\right)\right] \tag{3-16}$$

Cauchy's principal value of integral must be taken at $\theta=\theta_0$. Evaluation of the integrals in Eq. (3–16) yields for the velocity potential on the horizontal wing surface.

$$\varphi(\theta)=-\frac{V\delta_e}{\pi}\left[-2a\tanh^{-1}\left(\frac{\sin\theta}{\sin\mu}\right)\right.$$
$$\left.+2\cos\theta\tanh^{-1}\left(\frac{\tan\theta}{\tan\mu}\right)+\pi\left(1+\frac{2\mu}{\pi}\right)\sin\theta\right] \tag{3-17}$$

This formula was originally obtained by Dugan (Ref. 5). We define for the sake of simplicity, a new variable

$$Y=\cos\theta \tag{3-18}$$

The velocity component $v$ on the wing surface can be deried by differentiating $\varphi$ by $y$ and the result is

$$v=\frac{\partial\phi}{\partial\varphi}=-\frac{V\delta_e}{\pi}\frac{\sqrt{Y^2-a^2}}{Y+\sqrt{Y^2-a^2}}\left\{2\tanh^{-1}\left[\frac{a}{Y}\sqrt{\frac{1-Y^2}{1-a^2}}\right]\right.$$
$$\left.-\pi\left(1+\frac{2}{\pi}\mu\right)\frac{Y}{\sqrt{1-Y^2}}\right\} \tag{3-19}$$

The curves of velocity distribution $v(y)$ are shown in Figs. (2–1$\sim$3), where parameter $\lambda$ is the ratio of a semi-span to body radius $a$.

*Case-2* In order to calculate the coupling moment in roll induced by elastic deflection of wing due to crossflow, let us analyse the deflection angle of a elastic, supersonic wing fixed at the wing root, and twisted by uniform flow. The flow is assumed to be steady so that the wing panel is in equilibrium condition. The rigidity of material of wing panel is assumed to be constant in $x$ and $y$ directions. We denote chord length, nondimensional distance of center of pressure from elastic axis and the torsional rigidity of wing panel about the elastic axis by $c$, $e$ and $GJ$, as shown in Fig. (1–5).

The fundamental equation determining the twisted angle distribution of a wing panel is

$$\frac{d}{dy}\left(GJ\frac{d\delta}{dy}\right)=-q_0c^2eC_{L_\alpha}(\alpha+\delta) \tag{3-20}$$

The boundary conditions at the root and tip of the wing are

$$\delta=0 \quad \text{at} \quad y=a, \qquad \frac{d\delta}{dy}=0 \quad \text{at} \quad y=S \tag{3-21}$$

Now we assume that the wings are rectangular and the rigidity of wing panel is constant. We define $\Lambda$ by $\Lambda^2=q_0c^2eC_{L\alpha}/GJ$, then the solution of Eqs. (3–20), (3–21) is

$$\delta(y)=\alpha[\tan \Lambda(s-a) \sin \lambda y+\cos \Lambda y-1] \tag{3-22}$$

By this equation it is seen that the angle of elastic deflection is sinusoidally distributed. Stream function $\phi$ is given from Eqs. (3–1), (3–10) as:

$$\phi=-V_0\alpha\left\{-\frac{1}{\Lambda} \tan (s-a) \cos \Lambda(y_0-a)+\frac{1}{\Lambda} \sin \Lambda(y_0-a)-y_0\right\} \tag{3-23}$$

The rigidity of the wing material is usually chosen sufficiently large so as to avoid the wing panel flutter. Therefore, if $\Lambda$ is assumed to be sufficiently small compared to unity, we can expand Eq. (3–23) in the power series of $(y_0-a)$ as follows;

$$\phi=-V_0\alpha\{K_1(y_0-a)^2+K_2(y_0-a)^3+\cdots\} \tag{3-24}$$

where

$$K_1=\frac{\Lambda^2}{2}(s-a), \qquad K_2=-\frac{\Lambda^2}{6}(s-a),$$

By use of this equation we can solve Eq. (3–14) in an analytical form. We can obtain the stream function $\phi(y_0)$ in the form of power series of $(y_0-a)$ for a more general shape of wing if we know the wing deflection angle $\delta(y_0)$. Therefore the present analysis is applicable to the case of a more general shape of wing by determining the suitable values of $K_1, K_2, \cdots$. If we use the Eq. (3–24) to the first order, the stream function for the case–2 can be obtained by

$$\phi=K_1(y_0-a)^2 \tag{3-25}$$

Eq. (3–25) can be expressed in terms of $\theta_0$ by transformation relation Eq. (3–1), and we have

$$\phi(\theta_0)=K_1(\cos \theta_0+\sqrt{\cos^2 \theta_0-\cos^2 \mu}-\cos \mu)^2 \tag{3-26}$$

As the stream function $\phi(\theta_0)$ for the case-2 is obtained, the complex potential can be calculated in the same way as in the case-1. The stream function $\phi$ is zero at the root of the wing, so the first term of the left side of Eq. (3–14) is dropped for the present case.

The velocity potential is also calculated just in the same way as in case-1, but the integration is not limited to the elementary functions. Elliptic integrals which appear because of the distribution of varying strength of source and sink on the circumference of circle, plays important role in this case. Cauchy's principal value

is, of course, taken in integration. After tedious calculation (Appendix) the velocity potential is given by:

$$\begin{aligned}\varphi(\theta)=&-K_1\left(\frac{4\sin\theta}{\pi}\right)\left\{\sin\mu+\frac{\cos^2\theta}{\sin\theta}\tanh^{-1}\left(\frac{\sin\theta}{\sin\mu}\right)\right.\\&-\cos\mu\left[\mu+\cot\theta\tanh^{-1}\left(\frac{\tan\theta}{\tan\mu}\right)+\frac{\pi}{2}\right]\\&-K(\sin\mu)\cot\theta\,(\sin^2\mu-\sin^2\theta)^{1/2}\left[E\left(\sin^{-1}\left(\frac{\sin\theta}{\sin\mu}\right),\sin\mu\right)\right.\\&\left.\left.-\frac{E(\sin\mu)}{K(\sin\mu)}F\left(\sin^{-1}\left(\frac{\sin\theta}{\sin\mu}\right),\sin\mu\right)\right]\right.\\&\left.+K(\sin\mu)(\sin^2\mu-\sin^2\theta)+E(\sin\mu)\right\}\end{aligned}\tag{3-27}$$

where $K(k), E(k), F(\phi, k)$ and $E(\phi, k)$ denote complete elliptic integral of the first kind, the second kind, elliptic integral of the first kind and the second kind in Jacobi's form.

The velocity distribution is obtained by differentiating Eq. (3–27) by $y$, and the result is

$$\begin{aligned}v_1=\frac{d\varphi}{dy}=&-\frac{4}{\pi}\frac{1}{Y+\sqrt{Y^2-a^2}}\sqrt{\frac{Y^2-a^2}{1-Y^2}}\left\{\left[a\left(\frac{\pi}{2}+\cos^{-1}a\right)-2\sqrt{1-a^2}\right]Y\right.\\&+\sqrt{1-Y^2}\left[2Y\tanh^{-1}\sqrt{\frac{1-Y^2}{1-a^2}}-a\tanh^{-1}\sqrt{\frac{a^2(1-Y^2)}{(1-a^2)Y}}\right]\\&+K(\sqrt{1-a^2})\left[-2Y^3+(a^2+2)Y+(a^2-2Y^2)\sqrt{\frac{1-Y^2}{Y^2-a^2}}\right.\\&\left.\times E\left(\sin^{-1}\sqrt{\frac{1-Y^2}{1-a^2}},\sqrt{1-a^2}\right)\right]-E(\sqrt{1-a^2})\left[2Y\right.\\&\left.\left.+(a^2-2Y^2)\sqrt{\frac{1-Y^2}{Y^2-a^2}}F\left(\sin^{-1}\sqrt{\frac{1-Y^2}{1-a^2}},\sqrt{1-a^2}\right)\right]\right\}\end{aligned}\tag{3-28}$$

The curves of velocity distribution $v$ are shown in Fig. (2–4~6) through the parameter $\lambda$.

In the calculation stated above, the first term of the expansion (3–24) is used for determining $\phi$. It is also possible to include higher terms in (3–24) and the calculation can be performed in the same way. We have obtained the velocity distribution $v$ including the second term of (3–24). This approximation corresponds to quadratically increasing doublet on the wing panel. The induced velocity distribution for this case is given by

$$\begin{aligned}v_2=&-\frac{2}{\pi}\frac{1}{Y+\sqrt{Y^2-a^2}}\sqrt{\frac{Y^2-a^2}{1-Y^2}}\left\{6Y(1-2Y^2)\cos^{-1}a\right.\\&\left.+[6a\sqrt{1-a^2}-3\pi(2Y^2-1)]Y\right.\end{aligned}$$

$$
\begin{aligned}
&+12Y^2\sqrt{1-Y^2}\tanh^{-1}\left[\frac{a}{Y}\sqrt{\frac{1-Y^2}{1-a^2}}\right]\\
&-12aY\sqrt{1-Y^2}\tanh^{-1}\sqrt{\frac{1-Y^2}{1-a^2}}\\
&-6a\Big[K(\sqrt{1-a^2})(-2Y^3+(a^2+2)Y\\
&+(a^2-2Y^2)\sqrt{\frac{1-Y^2}{Y^2-a^2}}E\left(\sin^{-1}\sqrt{\frac{1-Y^2}{1-a^2}},\sqrt{1-a^2}\right)\\
&-E(\sqrt{1-a^2})(2Y+(a^2-2Y^2)\sqrt{\frac{1-Y^2}{Y^2-a^2}}F\left(\sin^{-1}\sqrt{\frac{1-Y^2}{1-a^2}},\sqrt{1-a^2}\right)\Big]\Big\}
\end{aligned}
\tag{3-29}
$$

From Eqs. (3–28), (3–29) $v_{\delta_e}$ for the second approximation which satisfy the boundary conditions at $y=a$ and $y=s$ can be obtained by choosing suitable value of $K_1$ and $K_2$. The results are also shown in Figs. (2–7～9).

## 4. Numerical Calculation of the roll Coupling Moment

The local pressure on the wing panel can be derived by calculation the cross product of the velocity components $v_{\delta_e}$ induced by wing deflection and the velocity components $v_\beta$ induced by crossflow. As the velocity components $v_\beta$ depends upon the number of wings because of wing panel interference, two typical cases are considered in this paper: one is planar wing-body combination and the other is cruciform wing-body combination. Some characteristic pressure distributions are shown in Fig. (3–1～6) for the two cases.

The coupling moment in roll can be calculated by integrating on the wing panel the product of the local pressure difference and the distance from the body axis.

$$
\begin{aligned}
M&=2c\int_a^s [P]ydy\\
&=8qc\int_a^s (1-v_\beta^+)v_{\delta_e}^+ydy
\end{aligned}
\tag{4-1}
$$

Though the integrated function diverges at the tip of wing due to $\sqrt{1-Y}$ in the denominator, as shown in Fig. (2–1～9), the value of integral can be proved to be finite because of finiteness of numerator in the integral interval. Numerical integration is performed in practice to attain the value of integral. To avoid slow convergence in integration due to the singularity existing at the tip of wing, we have divided the integral domain into two parts.

$$
\int_a^1 \frac{f(Y)}{\sqrt{1-Y}}dY=\int_a^{1-\varepsilon}\frac{f(Y)}{\sqrt{1-Y}}dY+\int_{1-\varepsilon}^1\frac{f(Y)}{\sqrt{1-Y}}dY \tag{4-2}
$$

where $\varepsilon$ is a very small parameter compared to 1. The first integral is calculated by numerical integration and the second integral is to be calculated by expanding

the numerator of Eq. (4–2) at $Y=1$ and then integrate each term separately.

$$I=\int_{1-\varepsilon}^{1}\frac{a_0+a_1(Y-1)+\cdots}{\sqrt{1-Y}}dY$$
$$=2a_0\varepsilon^{1/2}-\frac{2}{3}a_1\varepsilon^{3/2}+\cdots \tag{4–3}$$

Expansion is limited to certain order in practice by choosing a suitable value of $\varepsilon$.

The coupling moment appears as the second order product of $v_{\delta_e}$ and $v_\beta$, so a suitable definition of the moment coefficient should be considered. We define the coupling moment coefficient as the second derivative of $C_l$, the moment coefficient, by $\beta$ and $\bar{\delta}_e$ as follows:

$$C_l=\frac{M}{2q_0As}$$
$$C_{l_{\beta\delta_e}}=\frac{\partial^2 C_l}{\partial\beta\partial\bar{\delta}_e}=\frac{C_l}{\beta\bar{\delta}_e}=\frac{4}{s(s-a)}\int_a^s(1-v_\beta^+)v_{\delta_e}ydy \tag{4–4}$$

The coefficients are calculated and shown in Figs. (4–1~4). Simpson's 1/3 rule is chosen for the numerical integration mentioned above and a high speed computer HITAC 5020 is used. The value of $\varepsilon$ is changed from 0.1 to 0.001 to confirm the convergence of integral in equation (4–3). To ascertain the value of integrals we have continued to divide the interval of integral near the wing tip smaller and smaller and the extrapolated results have been compared to the one calculated by formula (4–3).

As can be seen by Fig. (1–3), the coupling moment depends upon bank angle $\chi$. The total coupling moment produced by crossflow and induced flow by wings for cruciform wing-body combination is given by adding torques on horizontal wings and vertical wings. For elastically deformed wings, the total coupling moment appears if there is, in any sense, difference between the horizontal and vertical wings. We have calculated $C_{l_{\beta\delta_e}}$ when span in horizontal wings $s_H$ is different from that of vertical wings $s_V$. In Figs. (4–3~4) $C_{l_{\beta\delta_e}}$ with unequal wing span is represented through the parameter $(s_V-a)/(s_H-a)$. When $(s_V-a)/(s_H-a)=0$, it corresponds to planar wing body combination and when $(s_V-a)/(s_H-a)=1$, it corresponds to cruciform wing body combination with equal span.

## 5. Results and Discussion

In Figs. (2–1~9) numerical results of velocity distribution $v_{\delta_e}$ on a wing panel are shown for various values of $\lambda$. All velocity $v_{\delta_e}$ is normalized by $\bar{w}$, which is span-wise averaged value of $w$ induced by doublet distribution. The extreme value of $\lambda$, such as 100, is also chosen, though it may be practically meaningless, in order to investigate the influence of span length and curvature of body on the velocity distribution.

Figs. (2–1~9) show that there is a singular point, as stated before in Chapter 3,

at the wing tip and $v_{\delta_e}$ is zero at the wing root to fulfil the boundary condition. It is also seen that all the $v_{\delta_e}$ are increasing function of $y$ except some region near wing root. The enlarged part of Fig. (2–1) shows that $v_{\delta_e}$ is negative near the wing root and the negative region increases when $\lambda$ increases. For example, the negative region is 1.4 times of body radius (16% of wing span) for $\lambda=10$ and 6.9 times of body radius (7% of wing span) for $\lambda=100$. Fig. (2–1) also shows that the absolute value of the negative peak is increasing function of $\lambda$. This trend of velocity profile can be explained by the fact that influence of wing tip on the velocity in the wing root region becomes small for large $\lambda$ and the influence of body curvature dominates in this region. For small $\lambda$ the appearance of negative region is limited in so small region that it can hardly be recognized. In the extreme case when $\lambda=\infty$, there should exist negative velocity from the root to the tip and when $\lambda=1$ there should be no negative region.

In Figs. (2–4~6) the velocity distributions of $v_{\delta_e}$ for case-2 are shown. The boundary conditions and parameter values are same as in case-1 but varying strength of doublet makes parallel flow component on wing surface and this is clearly seen in the existence of considerable wide negative region in the velocity distribution. In the first approximation of deflection angle of elastic wing when strength of doublet increases linearly in $y$ direction, this negative region is almost 57% of wing span for all $\lambda$ shown in Figs. (2–4~6). It can be said that $\lambda$ is not an essential parameter with respect to the negative velocity region for the case-2. In the second approximation of deflection angle of elastic wing when strength of doublet increases quadratically in $y$ direction the negative part is about 50% of wing span. Comparison with Figs. (2–4~6) shows, as can be expected, that the velocity curves slightly shift to the root.

Figs. (2–10~18) show the stream-lines on the wing panel for the case (1) and (2). Three values of $\lambda$, $\lambda=100$, 2, 1.1 are chosen for comparison.

Figs. (3–1~9) show the distribution of pressure difference (load) between upper and lower surfaces of wing panel. All value of pressure is normalized by the pressure $\beta\bar{\delta}_e q_0$. The results are shown for planar and cruciform wing-body combinations. As crossflow is interrupted by the vertical wing for cruciform wing-body combination, the resulting pressure is lower in comparison with that of planar wing-body combination. The difference of the load distribution between the two wing-body combinations become smaller as $\lambda$ decreases because body interruption effect becomes more important than wing interruption effect. It can be also seen that all the peaks of negative region in the load distribution slightly shift to wing tip as compared with that in velocity distribution. The shift is easily recognized for large $\lambda$. This is because the crossflow velocity $v_\beta$ is monotonously decreasing function of $y$ in $y>o$ and the difference in the shapes of pressure distribution and velocity distribution becomes remarkable when $\lambda$ becomes large.

Figs. (4–1~2) show the dependence of coupling moment coefficients $C_{l_{\beta\delta_e}}$ on $\lambda$ for case–1, and the results are shown for planar wing-body combination and cruciform wing-body combination for comparison. The curve shows the coupling

moment produced by two horizontal wing out of four wings in the cruciform wing-body combination. It is known that the coupling moment $C_{l_{\beta\delta_e}}$ is a decreasing function of $1/\lambda$. $C_{l_{\beta\delta_e}}=0$ when $\lambda=1$. This tendency can be explained by the fact that the crossflow velocity $v_\beta$ approaches to zero near the body and $C_{l_{\beta\delta_e}}$ produced by the coupling of $v_\beta$ and $v_{\delta_e}$ becomes smaller when $\lambda$ decreases. It can also be seen that $C_{l_{\beta\delta_e}}$ for cruciform wing-body combination is about 70% of $C_{l_{\beta\delta_e}}$ for the planar wing-body combination when $\lambda$ is large. But the differences decreases as $\lambda$ decreases and they are equally zero when $\lambda=1$.

In Fig. (4–2), $C_{l_{\beta\delta_e}}$ for case–2 are represented. The vertical ordinate also refers to $C_{l_{\beta\delta_e}}$ and horizontal abscissa to $1/\lambda$. The dotted lines represent the first approximation of the sinusoidal doublet distribution and real lines represent $C_{l_{\beta\delta_e}}$ for the second approximation. It is shown that general inclination of $C_{l_{\beta\delta_e}}$ curve is similar to that for case–1 and $C_{l_{\beta\delta_e}}$ value is smaller in case–2.

The value of $A$ is designed so small and corresponding deflection angle of wings are small except when wing divergence occurs. For example, if we assume the values of the constants as follows,

$$q_0=1.0\ \mathrm{kg/cm^2},\quad e=0.01,\quad C=1\ \mathrm{m},\quad C_{L_\alpha}=2,\quad GJ=0.89\times10^4\ \mathrm{kg/m^2}$$

we have

$$A^2=0.22\ \ 1/\mathrm{m^2}$$

For large $\lambda$ such as 100, Eq. (3–20) is no more valid. We have calculated $v_{\delta e}$ only to know the extreme case of body-span ratio, though it is practically meaningless.

In Figs. (4–3$\sim$4) $C_{l_{\beta\delta_e}}$ for cruciform wing-body combination with unequal span length are shown through the parameter $(s_V-a)/(s_H-a)$. $C_{l_{\beta\delta_e}}$ increases when $(s_V-a)/(s_H-a)$ decreases for a particular $s_H$ because cross flow become less interrupted. For constant $(s_V-a)/(s_H-a)$, $C_{l_{\beta\delta_e}}$ is of course decreasing function of $1/\lambda_H$. For constant $(s_V-a)/(s_H-a)$, it is shown that $C_{l_{\beta\delta_e}}$ has maximum value in $0<1/\lambda_H<1$. The maximum value of $C_{l_{\beta\delta_e}}$ is 1.5 when $1/\lambda_H=0.5$ for $(s_V-a)/(s_H-a)=2$ and it is 1.05 when $1/\lambda_H=0.65$ for $(s_V-a)/(s_H-a)=4$. The interruption effect of vertical wing is very effective for $(s_V-a)/(s_H-a)>1$ when $1/\lambda_H$ is small. When $(s_V-a)/(s_H-a)\to\infty$, $C_{l_{\beta\delta_e}}$ should go to zero.

The value of $C_{l_{\beta\delta_e}}$ here obtained for the cruciform wing corresponds to the roll coupling moment produced on the horizontal wing at the existence of the vertical wing, which acts only to interrupt the flow around the body. It should be remarked that no deflection of the vertical panel has been assumed in this calculation.

The roll coupling moment in the case where both horizontal and vertical wings are deflected can be obtained as the sum of each contribution:

$$C_{l\,\mathrm{total}}=C_{l_{\beta\delta_e}}\beta\delta_e+C'_{l_{\alpha\delta_e}}{}'\alpha\delta'_e$$

When the four wings have identical span, $C_{l_{\beta\delta_e}}$ is equal to $C'_{l_{\alpha\delta_e}}{}'$. Therefore, the roll moment will be produced in case–1 or in the case when there is any difference

in the cant angles of the horizontal and vertical wings. In case–2, however, the deflection takes place so as to satisfy the condition $\beta\delta_e = -\alpha\delta_e'$, therefore, $C_{l\,\text{total}}$ becomes equal to zero. We will compare $\beta$-$\delta_e$ coupling moment presented in this paper with the first order rolling moment by considering the flight condition of "Aerobee" at the burnout time. The rolling moment and the damping moment produced by cant angle of wings of the wing-body combinations are given in Ref. 2.

We will assume that $\lambda=0.4$ and the aspect ratio $A=4$ for brevity. By Ref. 5 flight conditions are given and the altitude is 40 Km, free stream velocity $v=2000\text{m/s}$ and roll frequency $r$ is 0.8 r.p.s. The rolling moment coefficients are given as follows:

| planar wing-body combination | cruciform wing-body combination |
|---|---|
| $C_{l\delta_a}= \quad 1.6$ | $C_{l\delta_a}= \quad 2.3$ |
| $C_{lP}=-1.0$ | $C_{lP}= \quad -1.6$ |

As shown in Fig. 1–7, the spin rate is very gradually increasing except few seconds after launching. $\beta$-$\delta_e$ coupling trerted in this paper appears under the roll-pitch resonance condition and it may be reasonable that the magnitude of the rolling moment should be compared with the summation of the first order rolling moments which are nearly in equilibrium condition.

The summation of the first order rolling moment is expressed as

$$C_l = C_{l\delta_a} \times \delta_a + C_{lP} \times \frac{2sr}{2v_0}$$

Here we set $s=0.75$ m, $\delta_a = 10' = 0.00145$ (rad) refering to the typical sounding rockets and we assume $\delta_e$ exists as malalignment of wing angle and that $\delta_e = 0.3\delta_a$. Then $C_l$ values are 0.0003 and 0.0002 for planar and cruciform configuration. The magnitudes of $\beta$-$\delta_e$ coupling moments are calculated by $C_{l\beta\delta_e} \times \beta \times \delta_e$ and we assume that $\beta=0.1$. Then $C_l$ values for case–1 are 0.0001 and 0.0002 for planar and cruciform configuration. The dynamic pressure is 0.05 kg/cm$^2$ at the burnout and $K_1=0.01$. $C_l$ value for case–2 is 0.0003 for planar configuration. The coupling moments calculated above are in the same order as the summation of the first order rolling moments.

The coupling moment for the cruciform configuration is considered to be one-tenth of this value, if the difference in the rigidities of the horizontal and vertical panels is assumed to be 10 percent, therefore, this is not so important as the moment caused by the wing angle malalignment. The burnout altitude of the solid-propellent rocket is usually smaller than the above-mentioned value and the dynamic pressure is in the order of a few kilograms per square centimeter. Therefore, even difference of several percent in th rigidities of horizontal and vertical wings can cause the roll-coupling moment in the same order as the summation of the first order rolling moment. The discussion stated above shows that coupling moment has considerable meaning in the flight of a rocket to which spin torque is produced by cant angle of wings when roll-pitch resonance occures. In the real

flight when the spin rate decreases a little, pitch angle varies and it will invite the serious results.

## 6. Conclusion

The rolling moment produced by the cross-coupling between the angle of attack or sideslip and the angle of the wing-panel deflection has been elucidated on the basis of the slender-body theory.

The formulas for the roll coupling moment coefficient have been derived for the planar- and cruciform-wing-body combinations in the two cases: 1) wing-panels canted, and 2) wing-panels deflected by aerodynamic load.

The roll dynamic coupling which occurs on the actual sounding rocket is a very complicated phenomenon, but the results of the present analysis will be useful in estimating the effect of individual factors, such as the differences in the wing size, aerodynamic characteristics and the difference in torsional rigidity of each panel.

The analysis of elastic deformation in this paper is essentially two-dimensional. This will be permitted as a rough approximation for taking into account the effect of wing deformation on the roll characteristics of the wing-body combination.

## Acknowledgement

The author would like to express his sincere gratitude to Professor F. Tamaki and Dr. M. Hinada for their instructive suggestions and helpful advices during the course of the present work.

*Department of Space Technology*
*Institute of Space and Aeronautical Science*
*University of Tokyo*
*November 1, 1972*

## References

[1] Nielsen, J. N.: Missile Aerodynamics, McGraw-Hill, 1960.
[2] Adams, G. J.: Theoretical Damping in Roll and Rolling Moment due to Differential Wing Incidence for Slender Cruciform Wings and Wing-Body Combinations, NACA TR 1088.
[3] King, L. V.: On the Direct Numerical Calculation of Elliptic Functions and Integrals, Cambridge, University Press, 1924.
[4] Ruth, C. E. and Rumbold, S. G.: Dynamic Roll Coupling. Proceedings of the Fifth International Symposium on Space Technology and Science, 1963.
[5] Dugan, D. W.: Theoretical Investigation on the Effects upon Lift of a Gap between Wing and Body of a Slender Wing-Body Combination, NACA TN 3224.
[6] Bisplinghoff, R. L.: Aeroelasticity, Addison-Wesley, 1957.
[7] Graham, E. W.: A Limiting Case for Missile Rolling Moments, Jour. Aero. Sci., Sept. 1951, pp. 624–628.

[8] Tucker, W. A. and Piland, R. O.: Estimation of the Damping in Roll of Supersonic-Leading-Edge Wing-Body Combinations, NACA TN 2151, 1950.
[9] Spreiter, J. R. and Sacks, A. H.: A Theoretical Study of the Aerodynamics of Slender Cruciform-Wing Arrangements and Their Wakes, NACA TR 1296, 1957.

TABLE 1 Types of coupling moment

| Horizontal Wing | | rolling moment |
|---|---|---|
| $Z_{\alpha\alpha}$ | $-4\alpha v_\alpha^+ v_\alpha^+$ | 0 |
| $Z_{\alpha\beta}$ | $4\alpha\beta(1-v_\beta^+)v_\alpha^+$ | |
| $Z_{\beta\delta_e}$ | $4\beta\delta_e(1-v_\beta^+)v_{\delta_e}^+$ | |
| $Z_{\beta\delta_a}$ | $4\beta\delta_a(1-v_\beta^+)v_{\delta_a}^+$ | 0 |
| $Z_{\delta_e\alpha}$ | $4\delta_e\left[\left(\frac{dz}{dx}\right)^+ - v_{\delta_e}^+ v_\alpha^+\right]$ | 0 |
| $Z_{\delta_a\alpha}$ | $4\delta_a\left[\left(\frac{dz}{dx}\right) - v_{\delta_a}^+ v_\alpha^+\right]$ | |

| Vertical Wing | | |
|---|---|---|
| $Y_{\beta\alpha}$ | $-4\beta w_\beta^+ w_\alpha^+$ | 0 |
| $Y_{\alpha\beta}$ | $-4\alpha\beta w_\beta^+(1+w_\alpha^+)$ | |
| $Y_{\beta\delta_e}$ | $-4\beta\delta_e w_\beta^+ w_{\delta_e}^+$ | |
| $Y_{\alpha\delta_a}$ | $-4\alpha\delta_a w_{\delta_a}^+(1+w_\alpha)$ | 0 |
| $Y_{\delta_a\alpha}$ | $-4\delta_a w_{\delta_a}^+ w_\alpha^+$ | |
| $Y_{\delta_a\delta_e}$ | $-4\delta_e\delta_a w_{\delta_a}^+ w_{\delta_e}^+$ | 0 |

## APPENDIX

Eq. (3–26) gives

$$\phi(\theta_0)=2K_1\{\cos^2\theta_0-\cos\mu\cos\theta_0+(\cos^2\theta_0-\cos^2\mu)^{1/2}(\cos\theta_0-\cos\mu)\} \quad \text{(A–1)}$$

Substituting Eq. (a–1) into Eq. (3–14) and considering $\phi(\mu)=0$ we can obtain the velocity potential $\phi(\theta)$:

$$\varphi(\theta)=\frac{4K_1\sin\theta}{\pi}(I_1+I_2+I_3+I_4) \quad \text{(A–2)}$$

where $I_1$, $I^2$, $_3$ and $I_4$ are given as follows:

$$\begin{aligned}
I_2&=\oint_0^{\mu}\frac{\cos^3\theta_0 d\theta_0}{\cos^2\theta-\cos^2\theta_0}\\
I_2&=-\cos\mu\oint_0^{\mu}\frac{\cos^2\theta_0 d\theta_0}{\cos^2\theta-\cos^2\theta_0}\\
I_3&=\oint_0^{H}\frac{(\cos^2\theta_0-\cos^2\mu)^{1/2}}{\cos^2\theta-\cos^2\theta_0}\cos^2\theta_0 d\theta_0\\
I_4&=-\cos\mu\frac{(\cos^2\theta_0-\cos^2\mu)^{1/2}}{\cos^2\theta-\cos^2\theta_0}\cos\theta_0 d\theta_0
\end{aligned} \quad \text{(A–3)}$$

The integrals $I_1$, $I_2$ and $I_4$ are expressed by the elementary functions.

$$\begin{aligned}
I_1&=-\sin\mu-\frac{\cos^2\theta}{\sin\theta}\tanh^{-1}\left(\frac{\sin\theta}{\sin\mu}\right)\\
I_2&=\cos\mu\left\{\mu+\cot\theta\tanh^{-1}\left(\frac{\tan\theta}{\tan\mu}\right)\right\}\\
I_4&=\frac{\pi}{2}\cos\mu
\end{aligned} \quad \text{(A–4)}$$

We write $\sin\theta_0=t$, then the integral $I_3$ is rewritten as

$$I_3=\oint_0^{t_\mu}\frac{(t_\mu^2-t^2)^{1/2}(1-t^2)^{1/2}}{t^2-\bar{t}^2}dt=\oint_0^{t_\mu}\frac{(t_\mu^2-t^2)(1-t^2)dt}{(t^2-\bar{t}^2)\sqrt{(t_\mu^2-t^2)(1-t^2)}} \quad \text{(A–5)}$$

where $t_\mu$ and $\bar{t}$ are defined by

$$\begin{aligned}
t_\mu&=\sin\mu\\
\bar{t}&=\sin\theta
\end{aligned} \quad \text{(A–6)}$$

The transformation of the integral $I_3$ into the standard form of the elliptic integrals gives

$$\begin{aligned}
I_3&=\int_0^{t_\mu}\left\{t^2+(\bar{t}^2-t_\mu^2-1)+(\bar{t}^2-t_\mu^2)(\bar{t}^2-1)\frac{1}{t^2-\bar{t}^2}\right\}\frac{dt}{\sqrt{(t_\mu^2-t^2)(1-t^2)}}\\
&=\int_0^{1}\left\{t_\mu^2x^2+c_1+c_2\frac{1}{1-(t_\mu^2/\bar{t}^2)x^2}\right\}\frac{dx}{\sqrt{(1-x^2)(1-t_\mu^2x^2)}}
\end{aligned} \quad \text{(A–7)}$$

where $c_1$, $c_2$ and $x$ are defined by

$$c_1=\bar{t}^2-t_\mu^2-1$$
$$c_2=(t_\mu^2-\bar{t})(1-1/\bar{t}^2)$$
$$x=t/t_\mu$$

The first term in Eq. (A–7) is expressed by use of the first complete integral $K(k)$ and the second complete integral $E(k)$ as follows:

$$\begin{aligned} t_\mu^2\oint_0^1\frac{x^2dx}{\sqrt{(1-x^2)(1-t_\mu^2x^2)}} &= t_\mu^2\oint_1^1\frac{[-(\sqrt{1-t_\mu^2x^2})+1]/t_\mu^2}{\sqrt{(1-x^2)(1-t_\mu^2x^2)}}dx \\ &= \oint_0^1\frac{dx}{\sqrt{(1-x^2)(1-t_\mu^2x^2)}} \\ &\quad -\oint_0^1\sqrt{\frac{1-t_\mu^2x^2}{1-x^2}}dx=K(t_\mu)-E(t_\mu) \end{aligned} \tag{A–8}$$

We denote the third kind of elliptic integral by $\Pi(\phi, k, n)$,

$$\begin{aligned} \Pi(\phi, k, n) &= \int_0^\phi\frac{d\phi}{(1+n\sin^2\phi)\sqrt{1-k^2\sin^2\phi}} \\ &= \int_0^{\sin^{-1}\phi}\frac{dx}{(1+nx^2)\sqrt{(1-x^2)(1-k^2x^2)}} \end{aligned} \tag{A–9}$$

where $\phi$ is an amplitude, $k$ is a modulus and $n$ is a parameter.

The integral $I_3$ is rewritten by use of Eqs. (A–7, (A–8) and (A–9) as

$$I_3=K(t_\mu)-E(t_\mu)+c_1K(t_\mu)+c_2\Pi\left(\frac{\pi}{2},\ t_\mu,\ -\left(\frac{t_\mu}{\bar{t}^2}\right)^2\right) \tag{A–10}$$

In the last term on the right hand of Eq. (A–10), we have that $n=-(t_\mu/\bar{t}^2)^2\leq -1$, which is called hyperbolic case. In the hyperbolic case of $\Pi(\phi, k, n)$, the parameter $n$ is conventionally rewritten by use of the function $sn$ of the complex argument as follows:

$$n=-k^2sn^2(\alpha+iK', k)=-1/sn^2(\alpha, k)$$
$$\text{where } 0<\alpha<K \text{ and } K'=K(\sqrt{1-k^2}).$$

For later convenience, we define $u$ by

$$u=F(\phi, k)$$

Then, the third incomplete elliptic integrals is rewritten in the alternative form:

$$\Pi(\phi, k, n)=\int_0^u\frac{du}{1+nsn^2(u, k)}=u-n\int_0^u\frac{sn^2(u, k)du}{1+nsn^2(u, k)}$$

$$=u+\int_0^u \frac{k^2sn^2(\alpha+iK', k)sn^2(u, k)}{1-k^2sn^2(\alpha+iK', k)sn^2(u, k)}du$$

$$=u+\frac{sn(\alpha+iK', k)}{cn(\alpha+iK', k)dn(\alpha+iK', k)}$$
$$\times\int_0^u \frac{k^2sn(\alpha+iK', k)cn(\alpha+iK', k)dn(\alpha+iK', k)sn^2(u, k)}{1-k^2sn^2(\alpha+iK', k)sn^2(u, k)}du$$

$$=u-\frac{sn(\alpha, k)}{cn(\alpha, k)dn(\alpha, k)}\int_0^u \frac{1}{2}k^2sn(\alpha+ik', k)sn(u, k)$$
$$\times\{sn(u+\alpha+iK', k)+sn(u-\alpha-iK', k)\}du$$

$$=u-\frac{sn(\alpha, k)}{cn(\alpha, k)dn(\alpha, k)}\int_0^u -\frac{1}{2}\{\mathcal{Z}(u+\alpha+iK', k)$$
$$-\mathcal{Z}(u-\alpha-iK', k)-\mathcal{Z}(\alpha+iK', k)+\mathcal{Z}(-\alpha-iK', k)\}du \quad \text{(A-11)}$$

where $\mathcal{Z}(\phi, k)$ is defined as $Z(\phi, k)=E(\phi, k)-\dfrac{E(k)}{K(k)}F(\phi, k)$

Then,

$$\pi(\phi, k, n)=u+\frac{1}{2}\frac{sn(\alpha, k)}{cn(\alpha, k)dn(\alpha, k)}\int_0^u \mathcal{Z}(u+\alpha+iK', k)$$
$$-\mathcal{Z}(u-\alpha-iK', k)-2Z(\alpha+iK', k)\}du$$

$$=u+\frac{1}{2}\frac{sn(\alpha, k)}{cn(\alpha, k)dn(\alpha, k)}\left\{-2\mathcal{Z}(\alpha+iK', k)u\right.$$
$$\left.+\int_0^u\left[\frac{d\log\Theta(u+\alpha+iK')}{du}-\frac{d\log\Theta(u-d-iK')}{du}\right]du\right\} \quad \text{(A-12)}$$

$$=u+\frac{1}{2}\frac{sn(\alpha, k)}{cn(\alpha, k)dn(\alpha, k)}\left\{-2\mathcal{Z}(\alpha+iK', k)u\right.$$
$$\left.-\left[\log\Theta(u+\alpha+iK')-\log\Theta(u-\alpha-iK')\right]_0^u\right\}$$

We have that

$$\mathcal{Z}(\alpha+iK', k)=\mathcal{Z}(\alpha)+\frac{cn\alpha dn\alpha}{sn\alpha}-\frac{1}{2}\pi iK \quad \text{(A-13)}$$

and

$$\Theta(u+iK')=iBH(u) \quad \text{(A-14)}$$

where

$$\log B=\frac{1}{4}\pi\frac{K'}{K}-\frac{1}{2}\pi i\frac{u}{K} \quad \text{(A-15)}$$

$H(u)$ is Jacobi's Theta-function given by the expansion

$$H(u)=2\sum_{n=0}^{\infty}(-1)^n \exp^{-\pi K'/K(n+1/2)^2}\sin\frac{2n+1}{2K}\pi u \qquad \text{(A-16)}$$

By Eq. (A-14), (A-15) we have

$$\log\Theta(u+\alpha+ik')-\log\Theta(u-\alpha-ik')=\log\left|\frac{H(u-\alpha)}{H(u+\alpha)}\right|-\pi i\frac{u}{K} \qquad \text{(A-17)}$$

In the hyperbolic case $\pi(\phi, k, n)$, i.e $n<-1$, the third elliptic integral is given by

$$\pi=-\frac{sn(\alpha)}{cn(\alpha)dn(\alpha)}\left[u\mathscr{Z}(\alpha)-\frac{1}{2}\log\left|\frac{H(u-\alpha)}{H(u+\alpha)}\right|\right] \qquad \text{(A-18)}$$

Considering $\left|\frac{H(K-\alpha)}{H(K+\alpha)}\right|=1$, the third complete elliptic integral $\pi\left(\frac{\pi}{2}, t_\mu-\frac{\bar{t}^2}{t_\mu^2}\right)$ is reduced to be

$$\begin{aligned}\pi\left(\frac{\pi}{2}, t_\mu, -\frac{\bar{t}^2}{t_\mu^2}\right)&=-\frac{sn(\alpha, t_\mu)}{cn(\alpha, t_\mu)dn(\alpha, t_\mu)}[K(t_\mu)\mathscr{Z}(\alpha, t_\mu)]\\&=-\frac{\sin\theta/\sin\mu}{\sqrt{1-\sin^2\theta/\sin^2\mu\cos\theta}}\left[K(\sin\mu)\mathscr{Z}\left(\sin^{-1}\left(\frac{\sin\theta}{\sin\mu}\right)\sin\mu\right)\right]\end{aligned} \qquad \text{(A-19)}$$

The third integral $I_3$ is expressed by use of Eqs. (A-10), (A-19) as follows:

$$\begin{aligned}I_3=&-(\sin^2\mu-\sin^2\theta)K(\sin\mu)-\mathrm{E}(\sin\mu)\\&+(\sin^2\mu-\sin^2\theta)^{1/2}\cot\theta\,K(\sin\mu)\\&\times\left[E\left(\sin^{-1}\left(\frac{\sin\theta}{\sin\mu}\right), \sin\mu\right)-\frac{E(\sin\mu)}{K(\sin\mu)}F\left(\sin^{-1}\left(\frac{\sin\theta}{\sin\mu}\right), \sin\mu\right)\right]\end{aligned} \qquad \text{(A-20)}$$

Thus, the velocity potential $\varphi(\theta)$ is given as:

$$\begin{aligned}\varphi(\theta)=&-\frac{4K_1}{\pi}\sin\theta\left\{\sin\mu+\frac{\cos^2\theta}{\sin\theta}\tanh^{-1}\left(\frac{\sin\theta}{\sin\mu}\right)\right.\\&-\cos\mu\left[\left(r+\frac{\pi}{2}\right)+\cot\theta\tanh^{-1}\left(\frac{\tan\theta}{\tan\mu}\right)\right.\\&+K(\sin\mu)(\sin^2\mu-\sin^2\theta)+E(\sin\mu)\\&-K(\sin\mu)(\sin^2\mu-\sin^2\theta)^{1/2}\cot\theta\\&\left.\left.\times\left[E\left(\sin^{-1}\left(\frac{\sin\theta}{\sin\mu}\right), \sin\mu\right)-\frac{E}{K}F\left(\sin^{-1}\left(\frac{\sin\theta}{\sin\mu}\right), \sin\mu\right)\right]\right\}\end{aligned} \qquad \text{(3-27)}$$

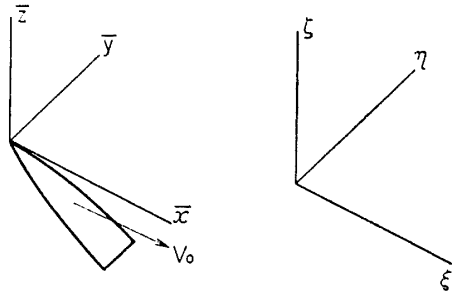


FIG. 1-1. Coodinate axes.

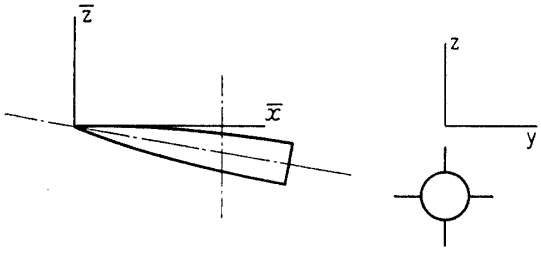


FIG. 1-2. Cross flow plane.

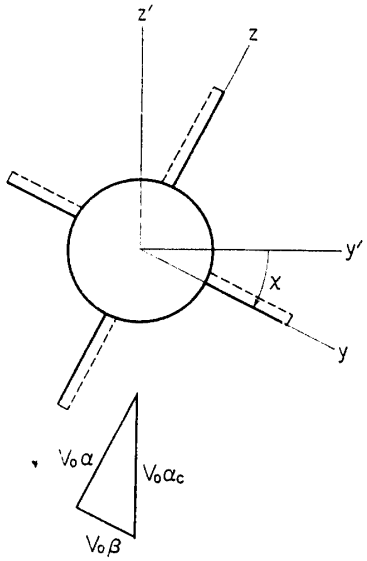


FIG. 1-3. Cruciform wing-body combination under pitch and bank.

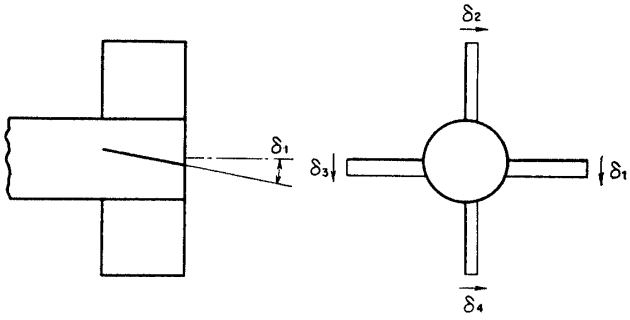


FIG. 1-4. Wing deflection angles.

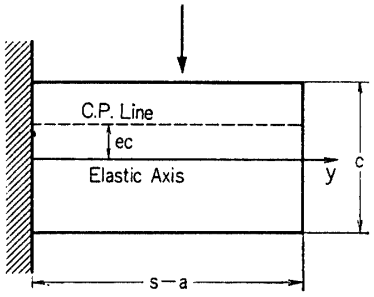


FIG. 1-5. Rectangular cantilrver wing.

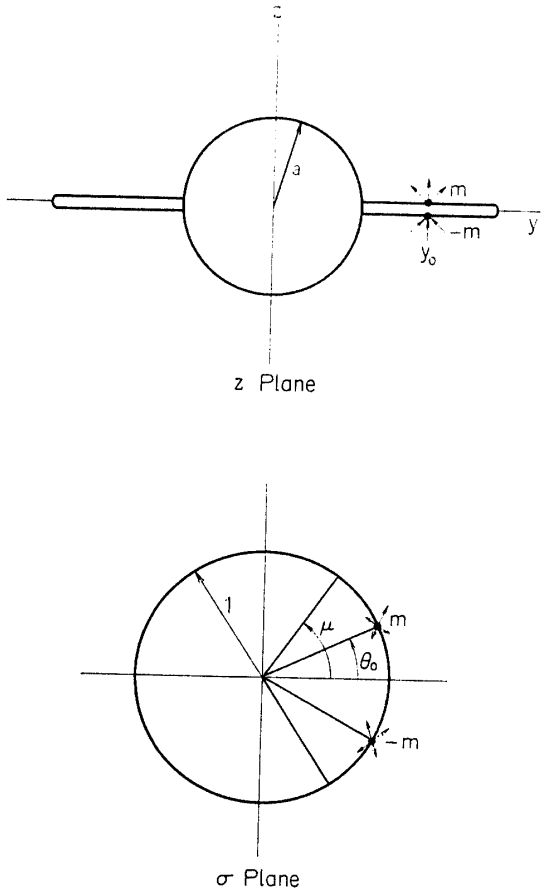


FIG. 1–6. Crossflow plane and transformed plane.

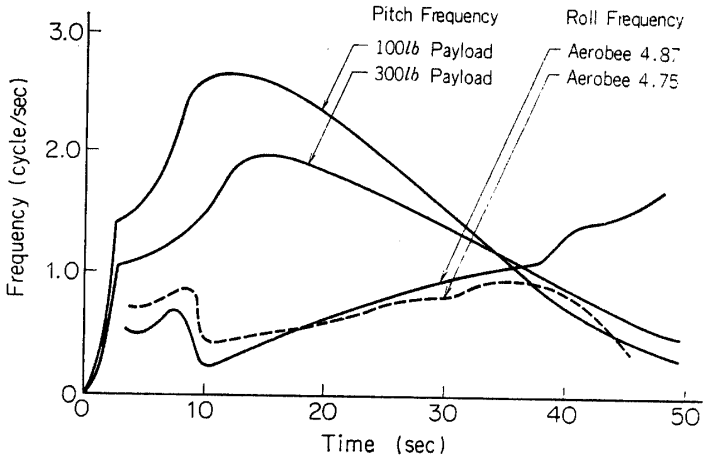


FIG. 1–7. Roll and pitch rates vs time Aerobee 4.75, 4.87 (NACA).

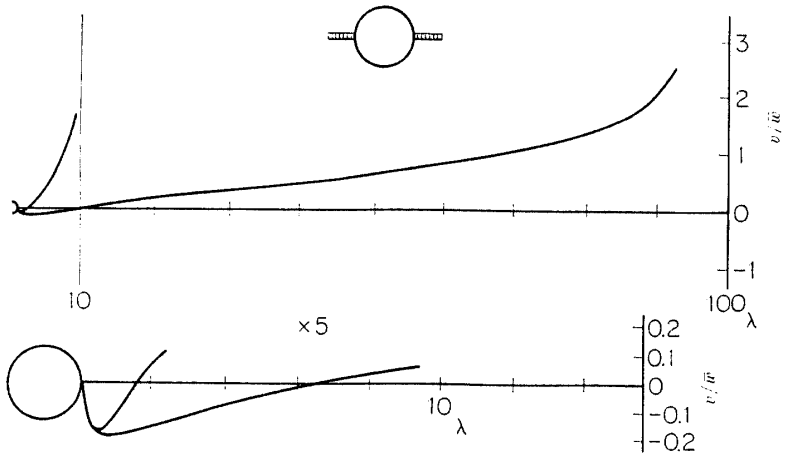


FIG. 2–1. Velocity distribution $v_{\delta_c}$ for a uniformly hinged wing.

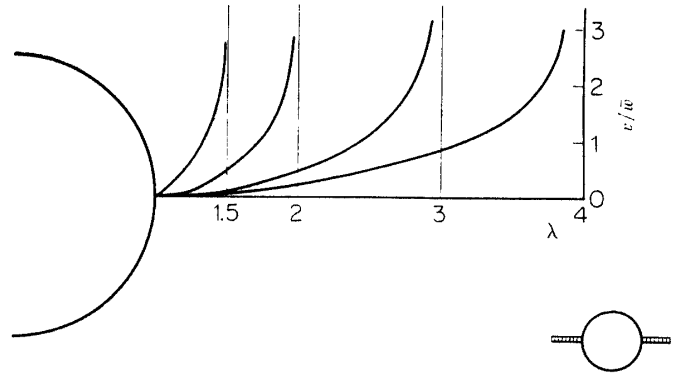


FIG. 2–2. Velocity distribution $v_{\delta_e}$ for a uniformly hinged wing.

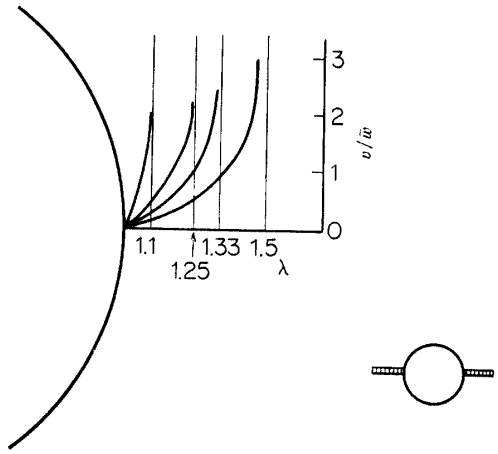


FIG. 2–3. Velocity distribution $v_{\delta_e}$ for a uniformly hinged wing.

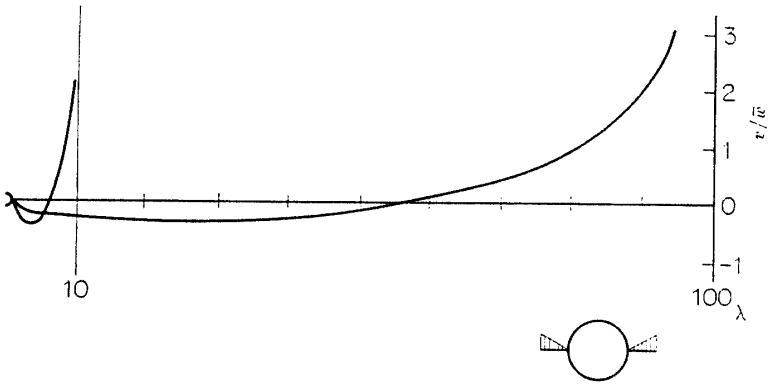


FIG. 2–4. Velocity distribution $v_{\delta_e}$ for a deflected wing. (first approximation)

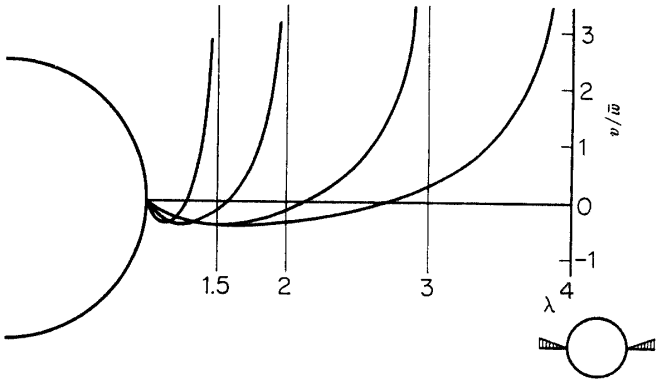


FIG. 2–5. Velocity distribution $v_{\delta_e}$ for a deflected wing. (first approximation)

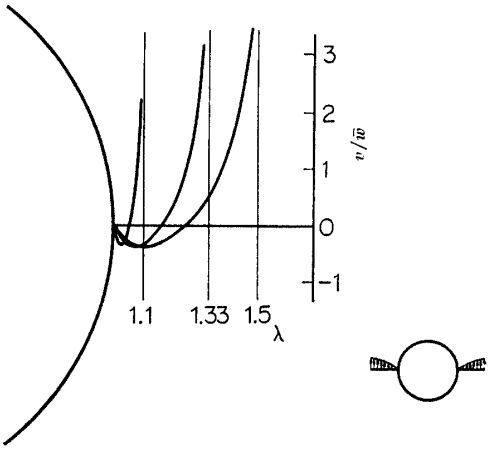


FIG. 2–6. Velocity distribution $v_{\delta_e}$ for a deflected wing. (first approximation)

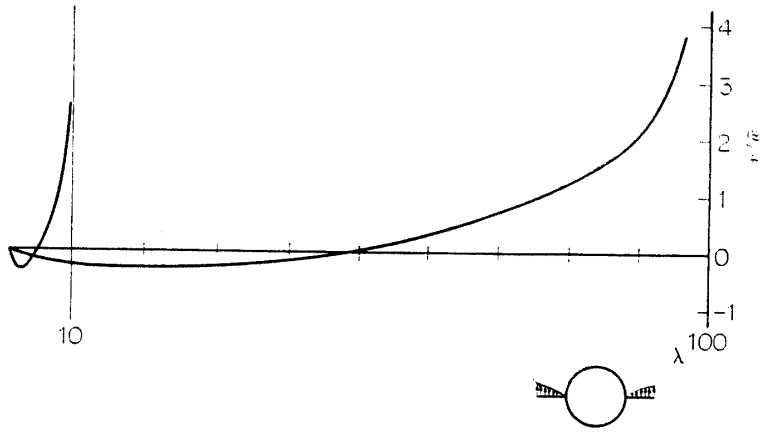


FIG. 2–7. Velocity distribution $v_{\delta_e}$ for a deflected wing. (second approximation)

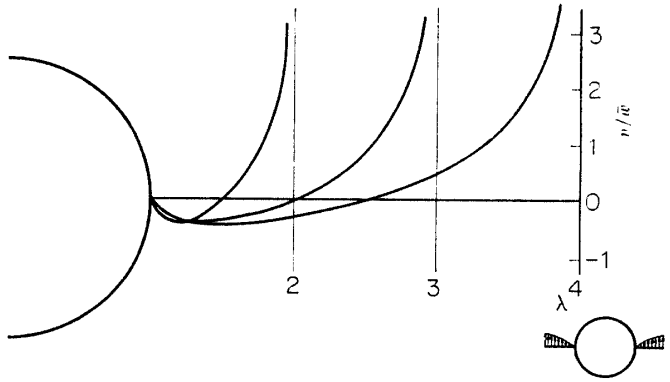


FIG. 2–8. Velocity distribution $v_{\delta_e}$ for a deflected wing. (second approximation)

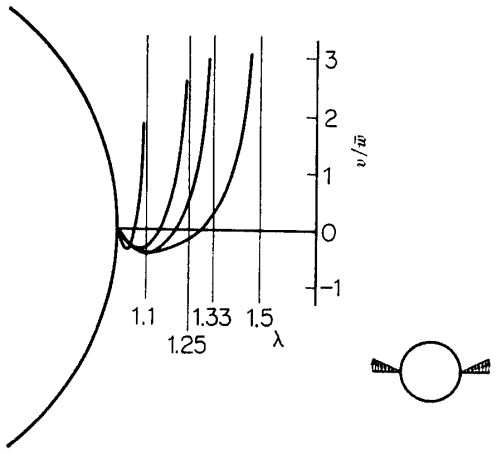


FIG. 2–9. Velocity distribution $v_{\delta_e}$ for a deflected wing. (second approximation)

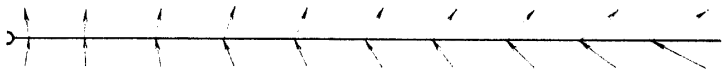

FIG. 2–10. Stream-line on the wing $\lambda=100$, case–1.

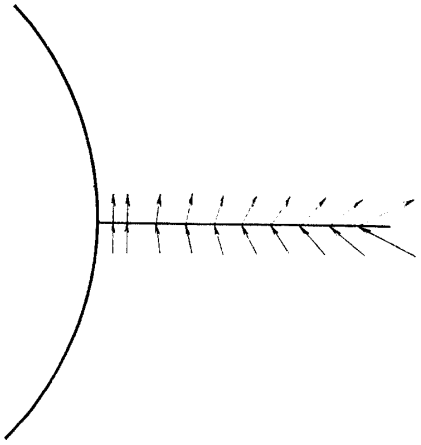

FIG. 2–11. Stream-line on the wing $\lambda=2$, case–1.

FIG. 2–12. Stream-line on the wing $\lambda=100$, case–2.
(first approximation)

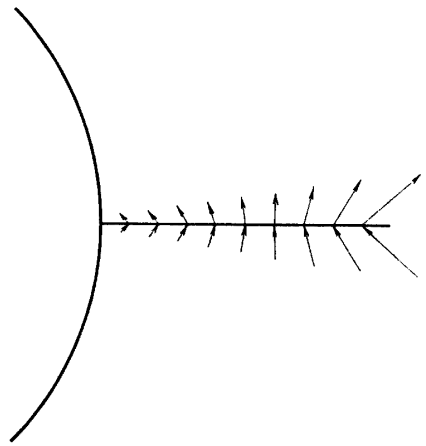

FIG. 2–13. Stream-line on the wing $\lambda=2$, case–2.

FIG. 2–14. Stream-line on the wing $\lambda=100$, case–2.

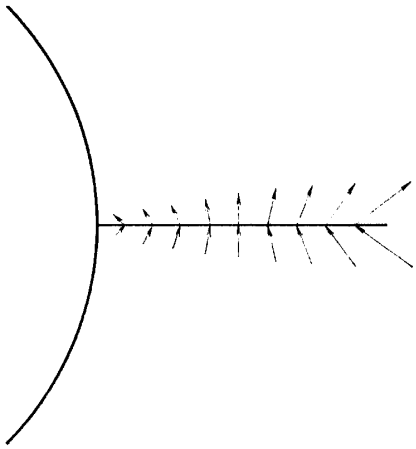

FIG. 2–15. Stream-line on the wing $\lambda=2$, case–2. (second approximation)

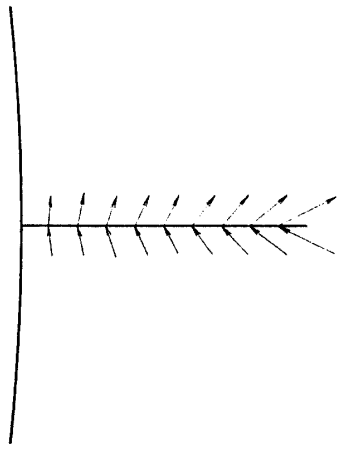

FIG. 2–16. Streamlines on the wing $\lambda=1.1$, case–1.

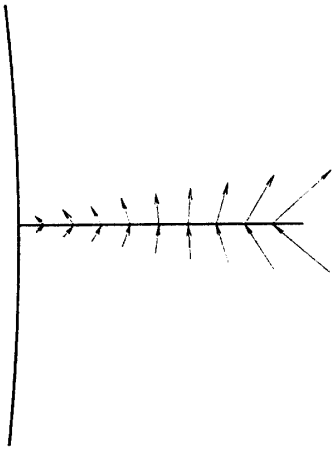

FIG. 2–17. Streamlines on the wing $\lambda=1.1$, case–2. (first approximation)

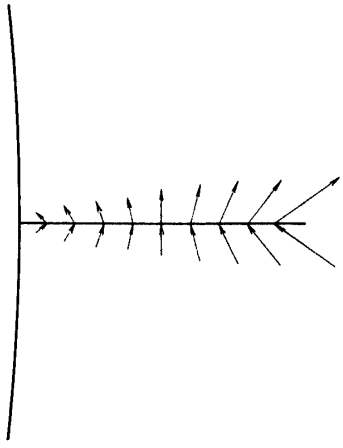

FIG. 2–18. Streamlines on the wing $\lambda=1.1$, case–2. (second approximation)

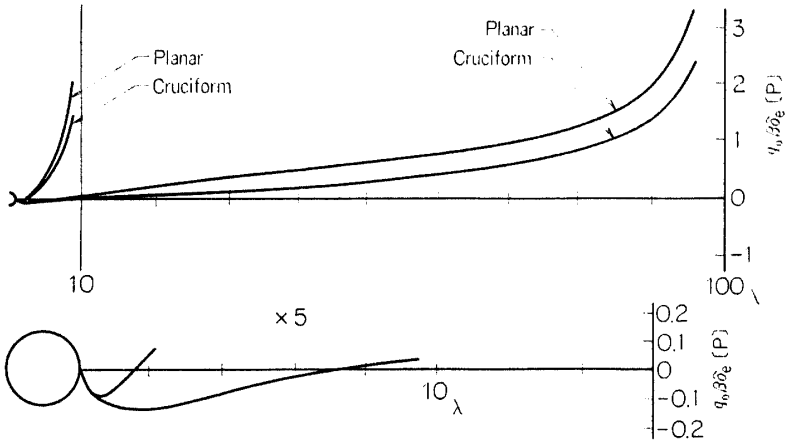


FIG. 3–1. Load distribution [*P*] for planar and cruciform wing-body combinations, case-1.

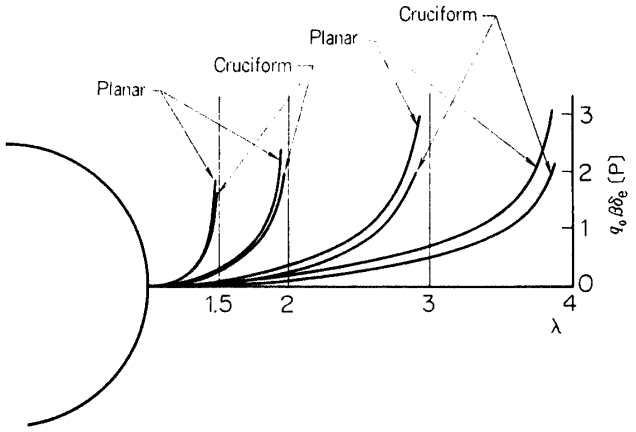


FIG. 3–2. Load distribution [*P*] for planar and cruciform wing-body combination.

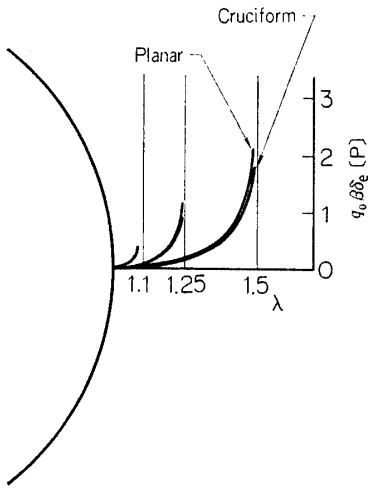


FIG. 3–3. Load distribution [*P*] for planar and cruciform wing-body combinations.

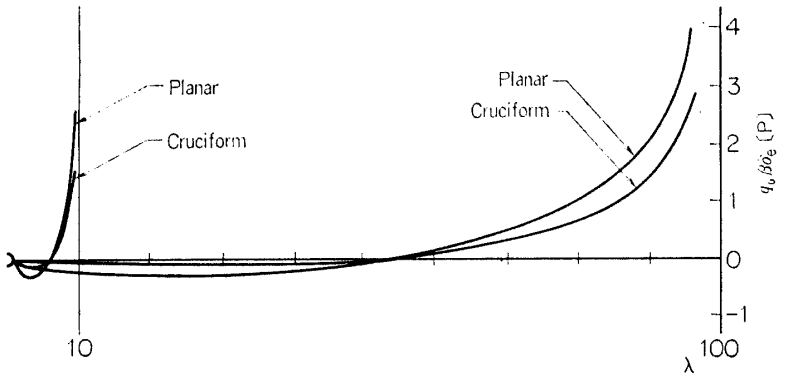


FIG. 3–4. Load distribution [*P*] for planar and cruciform wing-body combinations.

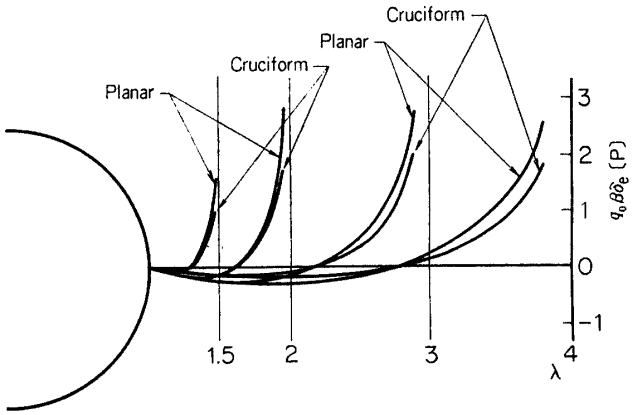


FIG. 3–5. Load distribution [*P*] for planar and cruciform wing-body combinations.

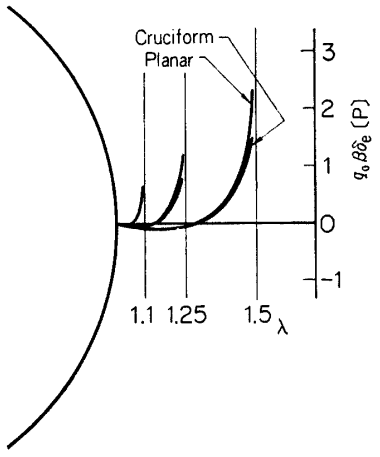


FIG. 3–6. Load distribution [*P*] for planar and cruciform wing-body combinations.

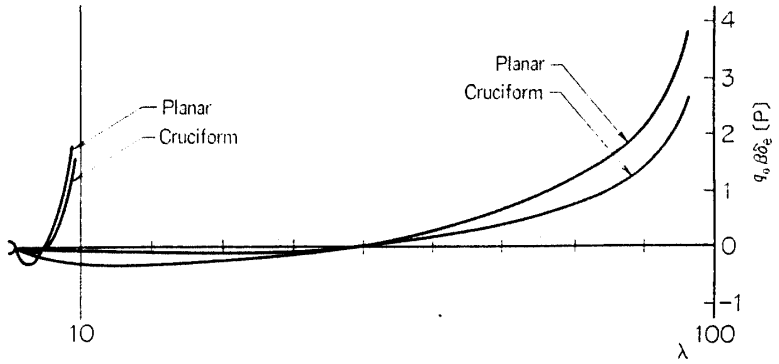


FIG. 3–7. Load distribution [$P$] for planar and cruciform wing-body combination case–2. (second approximation)

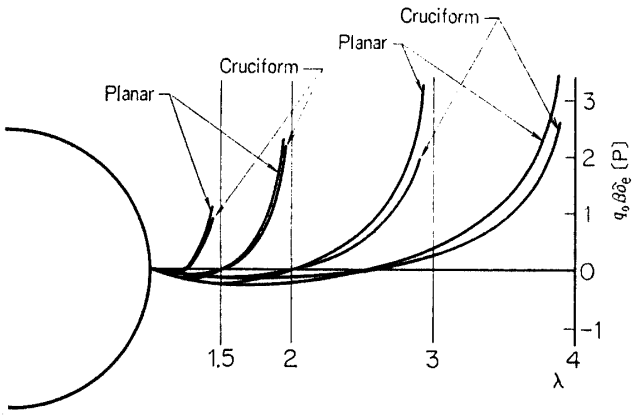


FIG. 3–8. Load distribution [$P$] for planar and cruciform wing-body combination case–2. (second approximation)

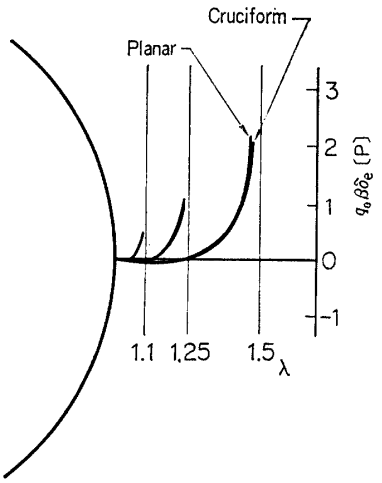


FIG. 3–9. Load distribution [$P$] for planar and cruciform wing-body combination case–2. (second approximation)

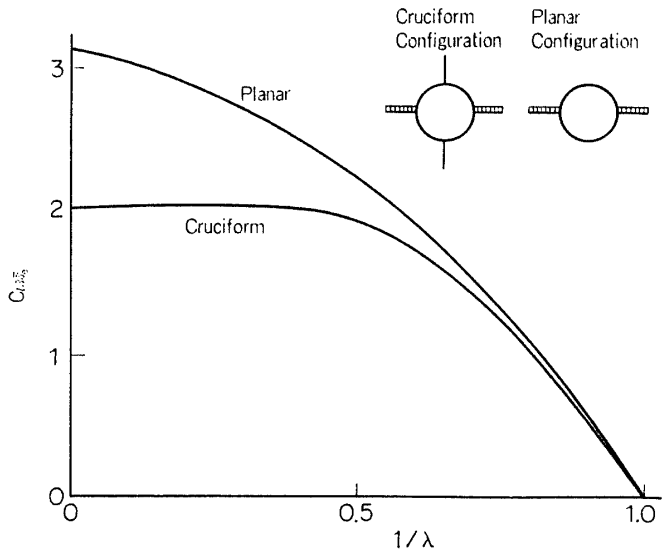


FIG. 4–1. Roll couping moment coefficient $C_{l_{\beta\delta_e}}$ for planar and cruciform wing-body combinations (1).

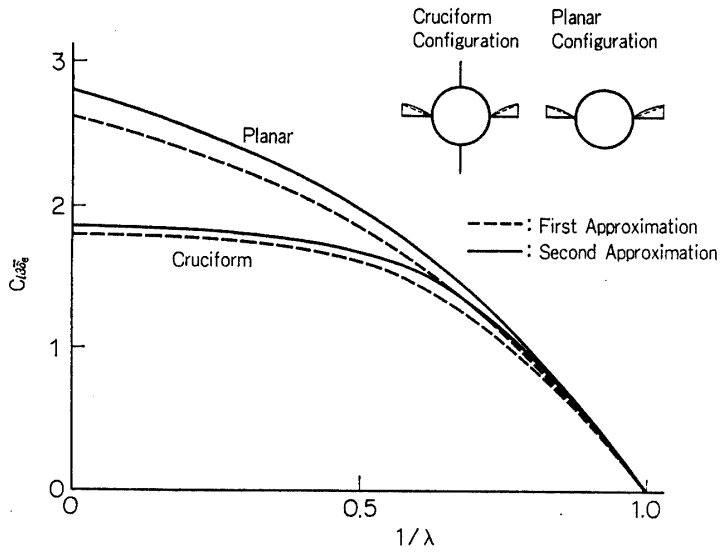


FIG. 4–2. Roll coupling moment coefficient $C_{l_{\beta\delta\delta}}$ for planar and cruciform wing-body combinations (2).

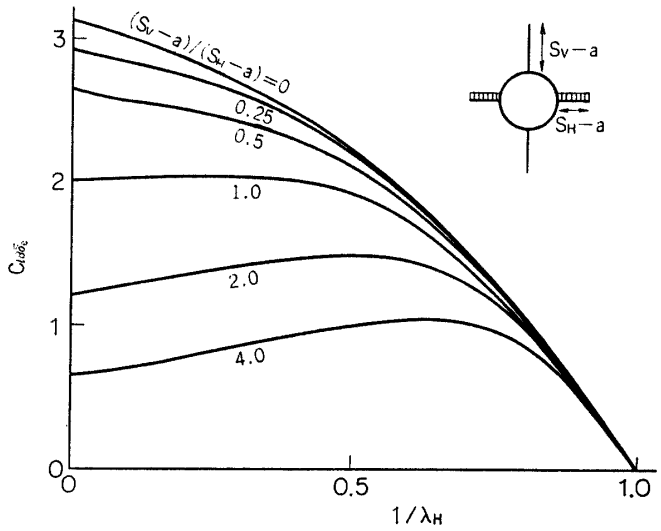


FIG. 4–3. Roll coupling moment coefficient $C_{l_\beta \delta_e}$ with unequal span length (1).

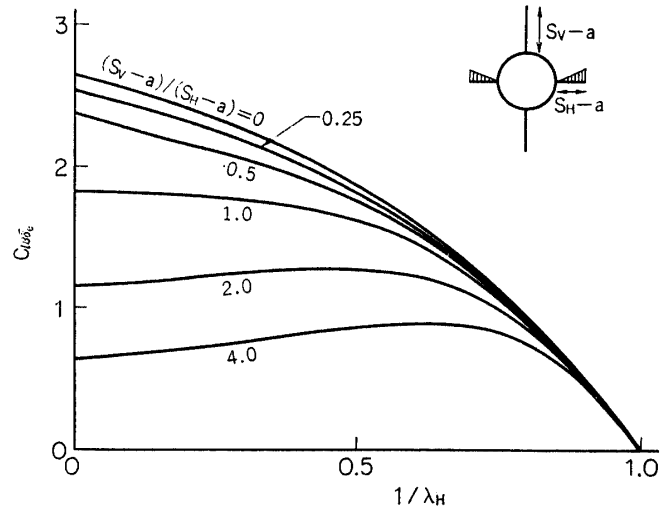


FIG. 4–4. Roll coupling moment coefficient $C_{l_\beta \delta_e}$ with unequal span length (2).

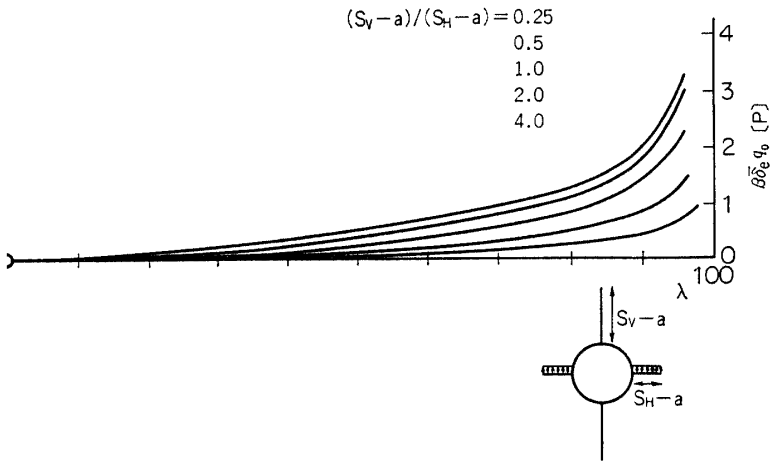


FIG. 4–5. Load distribution [$P$] for cruciform wing-body combination having unequal spans case–1.

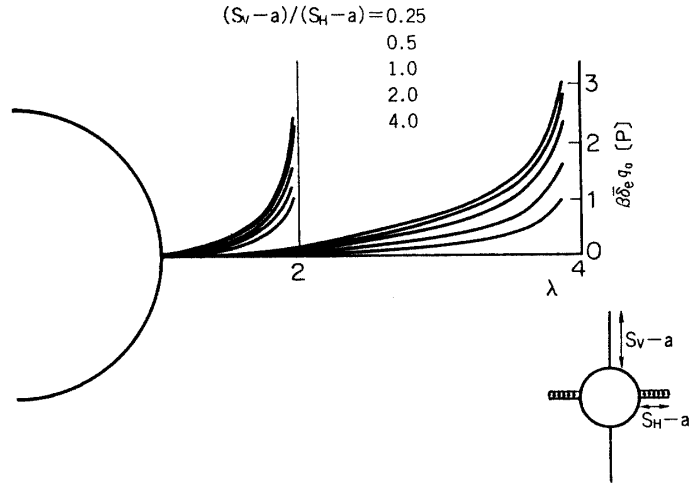


FIG. 4–6. Load distribution [*P*] for cruciform wing-body combination having unequal spans case–1.

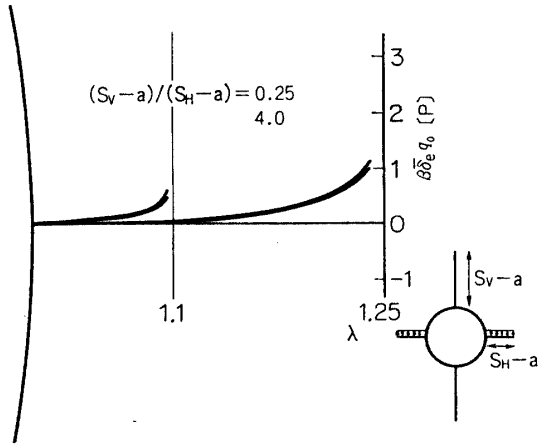


FIG. 4–7. Load distribution [*P*] for cruciform wing-body combination having unequal spans case–1.

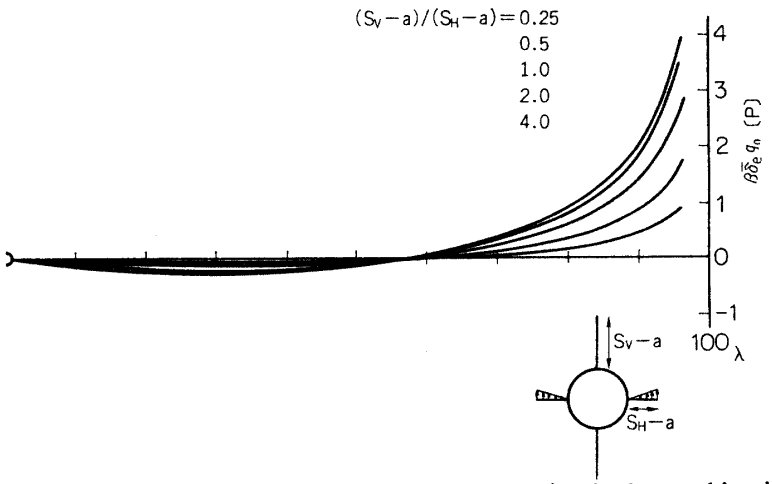


FIG. 4–8. Load distribution [*P*] for cruciform wing-body combination having unequal spans case–2.

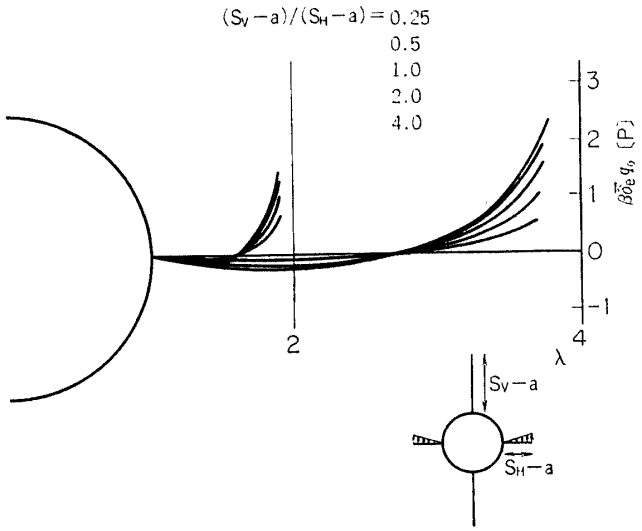


FIG. 4–9. Load distribution [*P*] for cruciform wing-body combination having unequal spans case–2.

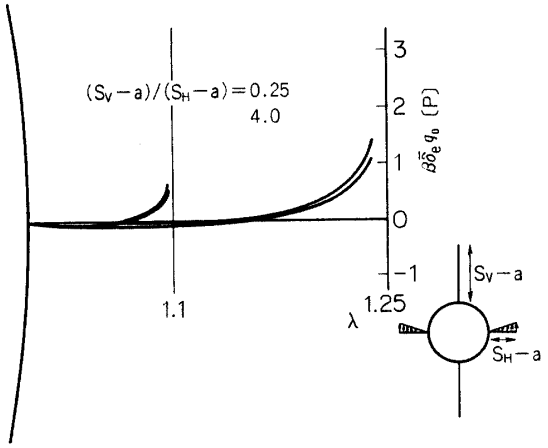


FIG. 4–10. Load distribution [*P*] for cruciform wing-body combination having unequal spans case–2.